The Karoo triple junction questioned: evidence from Jurassic and Proterozoic $^{40}Ar/^{39}Ar$ ages and geochemistry of the giant Okavango dyke swarm (Botswana).

F. Jourdan[a], G. Féraud[a,*], H. Bertrand[b], A.B. Kampunzu[c], G. Tshoso[d], B. Le Gall[d], J.J. Tiercelin[d], P.Capiez[b].

[a]*UMR-CNRS 6526 Géosciences Azur, Université de Nice-Sophia Antipolis, O6108 Nice, France*
[b]*UMR-CNRS 5570, Ecole Normale Supérieure de Lyon et Université Claude Bernard, 69364 Lyon, France*
[c]*Department of Geology, University of Botswana, Gaborone, Botswana*
[d]*UMR-CNRS 6538, Institut Universitaire Européen de la Mer, 29280, Plouzané, France,*

* Corresponding author. Fax: +33-4-92076816; E-mail: feraud@unice.fr

Abstract

The lower Jurassic Karoo-Ferrar magmatism represents one of the most important Phanerozoic continental flood basalt (CFB) provinces. The Karoo CFB province is dominated by tholeiitic traps and apparently radiating giant dyke swarms covering altogether ca. $3x10^6$ km^2. This study focuses on the giant N110°-trending Okavango dyke swarm (ODS) stretching over 1500 km across Botswana. This dyke swarm represents the main (failed) arm of the so-called Karoo triple junction that is generally considered as a key marker of the impingement of the Karoo starting mantle plume head. ODS dolerites yield six new plagioclase $^{40}Ar/^{39}Ar$ plateau (and mini-plateau) ages ranging from 178.7 ± 0.7 and 180.9 ± 1.3 Ma. The distribution of the ages along a narrow gaussian curve suggests a short period of magmatic activity centered around 179 Ma, i.e. ~5 Ma younger than the emplacement age of Karoo mafic magmas in the southern part of the Karoo CFB province (~184). This age difference indicates that Karoo magmatism does not represent a short-lived event as is generally the case for most CFB but lasted at least 5 Ma over the whole province. In addition, small clusters of plagioclase separated from twenty-eight other dykes and measured by "speedy" step-heating experiments (with mostly two to three steps), gave either "Karoo" or Proterozoic ages. Integrated ages of the Proterozoic rocks range from 851 ± 6 to 1672 ± 7 Ma, and one plateau age (959.1 ± 4.6 Ma) and one possibly geologically significant weighted mean age (982.7 ± 4.0 Ma) were obtained. Proterozoic and Karoo mafic rocks are petrographically similar, but Proterozoic dykes display clear geochemical differences (e.g. $TiO_2 < 2.1\%$) with the Karoo high-Ti ODS ($TiO_2 > 2.1\%$). Geochemical data combined with available Ar/Ar dates allow the identification of the two groups within a total set of seventy-seven dykes investigated: ~10 % of the bulk ODS dykes are Proterozoic. Thus, the Jurassic Karoo ODS dykes were emplaced along reactivated Proterozoic structures and there is no pristine Jurassic Nuanetsi triple junction as commonly proposed. This throws into doubt the validity of the "active plume head" Karoo CFB-rift models as being responsible for the observed "triple junction" dyke geometry.

Keywords: $^{40}Ar/^{39}Ar$ dating; geochemical discrimination; dyke swarm; triple junction; Karoo; mantle plume.

1. Introduction

Most of the Phanerozoic continental flood basalt provinces (CFB; e.g. Central Atlantic Province (CAMP), Karoo-Ferrar, Parana-Etendeka, Deccan) are associated with giant dyke swarms (i.e. >300 km; [1],[2]) with trends and geometry that are inferred to mark the response of the crust to plume-head impact. However, the possible role of inheritance of basement tectonic fabrics on the trend of the dyke swarms has not been properly documented. Specifically, it has never been clearly tested whether the three-branche dyke swarm system usually correlated with a rift triple junction are indeed neo-formed by a plume head impact or represent an artifact due to structural inheritance.

A crucial test for this question, provided that the dykes emplaced in basement are visible, is to determine if the dyke swarms contain old dykes (parallel to the main dyke swarm) indicating the polycyclic character of the lineament along which the dykes were emplaced.

Giant dyke swarms in southern Africa are good candidates for testing the role of inheritance during the emplacement of the Karoo large igneous province. The lower Jurassic Karoo-Ferrar magmatism (southern Africa and Antarctica) represents one of the most important Phanerozoic continental flood basalt (CFB) provinces. It is dominated by tholeiitic basalt traps and radiating giant dyke swarms. This igneous province covers ~$3x10^6$ km^2 and is usually linked to the disruption of Gondwana and the opening of the Indian Ocean. This study focuses on the giant Okavango dyke swarm (ODS) that stretches over 1500 km from Namibia to Zimbabwe through Botswana and displays a width of about 100 km (Figs.1-2), representing one of the most important fissural igneous complex in the world [1]. The ODS yielded few $^{40}Ar/^{39}Ar$ ages between 178.4 ± 1.1 Ma and 179.3 ± 1.2 Ma [3,4], with however one Proterozoic dyke identified in the swarm.

The goals of this study are the following: (1) to conduct additional high quality $^{40}Ar/^{39}Ar$ dating allowing to better constrain the age of the ODS emplacement; (2) to perform additional and numerous lower precision "speedy" step-heating experiments (which consist of analyzing a small number of steps) on small clusters of plagioclase in order to evaluate the proportion of Proterozoic dykes along the swarm, i.e. to test the possibility of inheritance; (3) to test a fast geochemical discrimination method between ODS Jurassic and Proterozoic dykes by comparing their ages and chemical composition in order to avoid systematic $^{40}Ar/^{39}Ar$ experiments on the whole dyke swarm and; (4) finally, to tentatively establish emplacement ages of these poorly studied Proterozoic intrusions.

2. Geological setting and sample description

The N110°-trending ODS cross-cuts Archaean rocks of the Zimbabwe craton, the metamorphic Limpopo-Shashe belt and the Karoo Permo-Jurassic sedimentary sequence exposed in northern Botswana (Fig. 1). The ODS includes hundreds of mostly vertical mafic dykes (thickness varies between 3 and 60m) mapped in detail using high-resolution aeromagnetic data [5]. Dyke exposures are generally very poor, but are excellent along major rivers such as the Shashe River near Francistown [4], which provides the opportunity to study a ~100 km long section across the ODS (Fig. 2). Along this section, about 150 dykes, intruding Archaean gneisses, were recorded in the field. Magnetic studies reveal more than 400 dykes buried under Quaternary sediments [6]. Thirty-one dykes and three sills were dated as part of this investigation. Thirty dykes and two sills are exposed along the Shashe River and one dyke and one sill are from the Tuli Basin (eastern Botswana). In addition, seventy-seven samples (including the dated samples) were analyzed for major elements and Zr (other trace elements will be published elsewhere). Proterozoic and Jurassic dykes are

indistinguishable in the field. For both geochronological and geochemical investigations, we selected all types of samples (fresh and altered), in order to get a more representative population of dykes.

All the samples yielding Jurassic ages show relatively uniform petrographic features. These are fine- to medium-grained dolerites with sub-ophitic, intergranular, or granular textures. Clinopyroxene and plagioclase are by far the most abundant minerals. Plagioclase (50-70 vol.%) occurs as microlites and sparse large (up to centimetric) zoned phenocrysts, sometimes clustered as glomerocrysts. Augite sometimes coexisting with pigeonite (30-40 vol.%) forms euhedral phenocrysts, glomerocrysts and subhedral granular aggregates. Olivine may occur in lesser amounts (up to 8% vol.%, e.g. samples Bot0028 and Bot0039). Fe-Ti oxides commonly form tiny grains or dendritic crystals in the groundmass. Interstitial glass and/or cryptocrystalline association of plagioclase and clinopyroxene are recorded in a few samples (e.g. Bot0091). Amphibole is rare and only observed in the small number of more evolved samples (e.g. Bot0089). Several samples contain variable amounts of secondary minerals such as sericite mainly infilling the plagioclase phenocrysts, and bowlingite, iddingsite or serpentine developed after olivine.

The samples yielding a Proterozoic age share petrographic features with the Jurassic dykes, with a paragenesis dominated by plagioclase and clinopyroxene (augite ± pigeonite). However, they are olivine-free and most of them contain interstitial micropegmatite, amphibole mostly replacing pyroxene (except Bot11, Bot0003 and Bot0035 which are amphibole free) and, in some cases, biotite. They are frequently altered into sericite, calcite, chlorite and kaolinite. Some of these samples tend to have a coarser-grained texture, compared to the Jurassic samples.

3. Analytical methods

A set of seventy-seven samples (including 8 samples previously analyzed by [4]) was selected for major and selected trace element analyses (Table 3, obtained in the background data set). They were crushed and powdered in an agate mill and analyzed by XRF (Philips PW 1404 spectrometer) at University of Lyon. Major and trace elements were determined on fused disc and pressed powder pellets, respectively. Analytical uncertainties vary from 1% to 2% and from 10% to 20% for major and trace elements respectively, depending on the concentration of the element.

Thirty-four hand-picked fresh plagioclase separates (10-30 grains for so-called "speedy" step heating experiments, defined below, and 30 mg for bulk sample analyses, fraction 150-300μm) were separated using a Frantz magnetic separator and then carefully selected under a binocular microscope. The samples were irradiated for 75.3 hours in the Hamilton McMaster University nuclear reactor (Canada) in position 5C along with Hb3gr hornblende neutron fluence monitor for which an age of 1072 Ma is adopted [7]. The total neutron flux density during irradiation was 9.0×10^{18} neutron/cm². The estimated error bar on the corresponding $^{40}Ar^*/^{39}Ar_K$ ratio is ±0.2% (1σ) in the volume where the samples were included. Small clusters of plagioclase (for step heating and "speedy" step heating experiments) were heated with a CO_2 Synrad 48-5 laser beam, and isotopic measurements were performed with a VG3600 mass spectrometer. Step heating experiments on plagioclase bulk samples were performed with a double vacuum high frequency furnace and the mass spectrometer is composed of a 120° M.A.S.S.E. tube, a Baur-Signer GS 98 source and a Balzers electron multiplier. The majority of samples were heated only with few steps with the aim of discriminating between Jurassic and Proterozoic dykes, and 9 samples (Bot0003-35-43-47-58-64-98-103-83) were step-heated in detail. The criteria to define a plateau age are (1) at least

70% of the ^{39}Ar released; (2) a minimum of three successive steps in the plateau; (3) the integrated age of the plateau should agree with each apparent age of the plateau within a two sigma confidence level (2σ). Plateau and integrated ages are given at the 2σ level (Table 1), but individual apparent ages are given at 1σ level (Table 2, obtained in the Background data set). The uncertainties on the $^{40}Ar/^{39}Ar$ ratios of the monitors are included in the calculation of the integrated and plateau age uncertainties but the error on the age of the monitor is not included in the calculation.

4. Results

4.1. Geochronology

In the "speedy" step-heating experiments that yielded Jurassic ages, a first step was performed to degas atmospheric and alteration phase argon. The second and third (when present) steps (including fusion) represent 83 to 95% of the radiogenic ^{40}Ar released (Fig. 3a). Seventeen samples yielded poorly defined second and third step ages between 175.4 ± 7.0 and 194.9 ± 6.6 Ma (Table 1), corresponding to a rather flat gaussian curve in an age-probability density distribution diagram with a peak-age at 180.4 Ma (Fig. 4).

Six plagioclase bulk samples yielded new precise data including four plateau ages (Bot0043, 47, 58, 103) and two mini-plateau ages (with 54.4 % and 50.0 % of ^{39}Ar released for sample Bot0064 and Bot0098, respectively), altogether ranging from 178.7 ± 0.7 Ma to 180.9 ± 1.3 Ma (Tables 1-2; Fig. 3b). $^{37}Ar_{Ca}/^{39}Ar_K$ ratio spectra associated with plateau ages display relatively regular undisturbed flat patterns, with values mainly ranging from 9.8 to 27, highlighting the negligible role of alteration phases in these ages. Lower apparent ages displayed by the sample Bot0098 and Bot0064, are linked to alteration phases as shown by the corresponding relatively low $^{37}Ar_{Ca}/^{39}Ar_K$ ratios (the low temperature steps excepted: see below). The fact that the mini-plateau ages correspond to the highest $^{37}Ar_{Ca}/^{39}Ar_K$ ratios lead us to conclude that these ages reflect fresh plagioclase, and therefore are probably valid, even if the plateau age criteria (given above) cannot be applied. The relationship between apparent ages and Ca/K ratios is not clear at low temperature, where the age spectra often begin by higher and decreasing apparent ages. This phenomenon was previously observed [4], and was explained by either excess argon (only present at low temperature) or by recoil of ^{39}Ar from potassic alteration phases. This last hypothesis is strengthened by the present data that show that the highest low temperature ages are displayed by plagioclase samples showing the lowest Ca/K ratios at low temperature (corresponding to the highest proportion of potassic alteration phases; cf. Bot0098 and Bot0064). The new data are similar to our previous plateau and integrated age determinations on the ODS [4], ranging from 178.4 ± 1.1 to 179.3 ± 1.2 Ma. Six previous and six new concordant plateau and mini-plateau ages range from 178.4 ± 1.1 and 180.9 ± 1.3 Ma and display a well defined gaussian curve when plotted in an age-probability density distribution diagram, with a peak at 179 Ma (Fig. 4). Data (plateau steps) were plotted on inverse correlation diagrams (i.e. $^{36}Ar/^{40}Ar$ vs. $^{39}Ar/^{40}Ar$) and yielded isochron ages between 178.7 ± 1.1 and 181.8 ± 2.0 Ma concordant with the plateau ages (error at 95 % confidence level; Table 1b). Initial $^{40}Ar/^{36}Ar$ values (233.4 ± 27.7 to 317.0 ± 86.9) are poorly defined due to a strong clustering of the data near the $^{39}Ar/^{40}Ar$ axis.

Eight dykes and three sills from the Okavango dyke swarm (including one sample Bot17 from [4]) display unambiguously Proterozoic ages (see discussion below) from all step-heating experiments. The integrated ages range from 851 ± 6 to 1672 ± 6 Ma, therefore showing a large age range that is probably not geologically significant. The sample Bot0003 was analyzed on both a bulk sample and a small cluster of about 30 grains more carefully

selected, and displayed different age spectra. The small cluster gave a less disturbed age spectrum with a plateau age at 959.1 ± 4.6 Ma that may be geologically significant because it corresponds to homogeneous $^{37}Ar_{Ca}/^{39}Ar_K$ ratios (Fig. 3b). Both the more disturbed $^{37}Ar_{Ca}/^{39}Ar_K$ ratio and the higher integrated age obtained on the bulk sample seem to indicate a substantial alteration coupled with some excess of argon (probably released at high temperature). The sample Bot0083 does not give a plateau age, but the flat section of apparent ages over 75.7% of ^{39}Ar released yields a weighted-mean age of 982.7 ± 4.0 Ma that may represent a meaningful age of this sample. The isochron diagrams provide no information on the age and the initial $^{40}Ar/^{36}Ar$ ratio because of a strong clustering of the data.

The results obtained on other samples by "speedy" step-heating experiments display Proterozoic ages, but are difficult to interpret in detail. It appears that the very variable apparent ages may be the result of both alteration (clearly visible on the analyzed samples that were locally milky, and demonstrated by variable $^{37}Ar_{Ca}/^{39}Ar_K$ ratios) and probably some excess argon. The two samples Bot0003 and Bot0083 excepted, it is therefore not possible to attribute precise ages to these Proterozoic samples.

4.2. Geochemistry

All the rocks investigated have a basaltic or basalt-andesitic composition (Fig. 5) according to the classification of Le Bas et al. [8]. They are quartz- or olivine- normative tholeiites. SiO_2 varies from 49.3 to 52.4 wt.%, MgO from 3.9 to 7.2 wt.% and K_2O from 0.3 to 2.2 wt.%. Two dykes (Bot0049 and Bot0089) are made of more evolved rocks containing 55.3 – 57.1 wt.% SiO_2, 2.5 wt.% MgO and 2.6 – 3.3 wt.% K_2O. These dolerites display tholeiitic trends characterized by increasing SiO_2, TiO_2 and Zr contents for decreasing Mg# [$Mg/(Mg+Fe^{2+})$] (Fig. 6). On the basis of the TiO_2 and P_2O_5 (and to some extent Zr) contents, the ODS displays two distinct populations: low-Ti/low-P and high-Ti/high-P. The low-Ti dolerites are characterized by TiO_2 values between 0.50-2.14 wt.%, P_2O_5 values between 0.06 and 0.23 wt.%, Zr values between 61 and 194 ppm, and mostly by a relatively high SiO_2 content (Fig. 6). The high-Ti dolerites contain 2.16-4.4 wt.% TiO_2, 0.23-1.00 wt.% P_2O_5 and 151-720 ppm Zr. There is a slight overlap between the two groups for Zr concentrations, whereas TiO_2 contents are quite distinct between the two groups (Fig. 6).

Based on the 43 dated samples (34 new data and 9 data from [4]), these two groups are also discriminated by their age, Jurassic for high-Ti and Proterozoic for low-Ti, respectively (Fig. 6), with a TiO_2 boundary at 2.15 wt% (Fig. 7).

The Proterozoic mafic dykes share chemical features with the low-Ti Karoo mafic rocks ([9],[10]) despite the fact they are chronologically distinct. These dykes can be subdivided into two sub-groups (< and > 1.5 %wt TiO_2, also discriminated by their SiO_2- Mg relationships (Fig. 6), the significance of these sub-groups being beyond the scope of this paper (work in progress).

5. Discussion

5.1. Timing of Karoo ODS emplacement

Six previous [4] and six new $^{40}Ar/^{39}Ar$ ages constrain precisely the Karoo ODS igneous event between 178.4 ± 1.1 Ma and 180.9 ± 1.3 Ma (2σ, including analytical errors only, see [12] for dating inter-comparison). All these ages are concordant and are distributed along a nearly Gaussian curve with a peak centered at 179 Ma and indicating a ca. 2.3 Ma magmatic activity at mid-height of the peak. This peak-age is similar to the plateau-ages (plagioclase separate)

of Karoo basalts exposed in northwestern Zimbabwe (179.2 ± 0.9 to 179.8 ± 1.2 Ma; [11]). These ages are ~5 Ma younger that the 184 Ma peak age of the southern Karoo magmatic province in South Africa, Lesotho and Namibia (Fig. 1 and 4) obtained using both plagioclase separates Ar/Ar (9 samples) [13] and zircon and baddeleyite U/Pb (1 sample) [14] dating techniques.

These data indicate a ~5 Ma diachronism between the southern (Lesotho, South Africa, Southern Namibia) and northern (Botswana, northwestern Zimbabwe) Karoo igneous province. This age difference cannot be attributed to analytical bias since Ar/Ar ages <180 Ma for the Zimbabwean basalts [11] of the northern province and the ca. 184 Ma mafic rocks from the southern province [13] were processed using the same procedure and the same flux monitor (FCT-3) for which an age of 28.02 Ma was adopted [15]. Furthermore, the age used for Hb3gr hornblende monitor (i.e. 1072 Ma) during this study and by Le Gall et al. [4] is in agreement with the result of intercalibrations performed with FCT-3 standard by Renne [15] and by us (in progress). Moreover, whereas systematic errors [12] (not included in our error bar calculation) are crucial for comparing our ages with U/Pb data, this is not the case for Ar/Ar ages (that represent the majority in Karoo) comparisons, if the monitor ages are well constrained.

In the "speedy" step-heating experiments, the second and third step ages display a wide and flat non-gaussian probability curve approximately centered on 180.4 Ma (indistinguishable at high confidence level from the plateau age peak at 179 Ma) which is likely to represent a complex mixture of (1) radiogenic argon from fresh plagioclase; (2) radiogenic argon from related secondary sericite and; (3) excess argon or an argon composition affected by a recoil of ^{39}Ar from secondary K-rich phases at low temperature (see above). This shows that the "speedy" step-heating does not yield precise ages, when compared to more classical step heating measurements, but the difference between the two peaks is <2 Ma (<1%) only. This slight difference may be the result of frequent anomalously old ages at low temperature that could not be removed with poorly detailed step heating experiments. Therefore, it appears that this fast technique represents an appropriate tool for discriminating Jurassic and Proterozoic dykes populations. This is strengthened by a statistical treatment that was performed on the integrated ages (i.e. equivalent to the conventional K/Ar method) obtained on samples giving plateau or mini plateau ages (n = 12: [4], and this work). The same sharp main peak at 179 Ma is obtained, although it is accompanied by a smaller secondary peak centered around 181.1 Ma (Fig 4). This second peak marks high ages obtained during low temperature steps (Fig. 3b).

5.2. Proterozoic versus Jurassic dyking: geochemistry as a discriminant tool

Despite the existence of excess argon detected on some samples (Bot0003 bulk sample and possibly Bot0094 and Bot11), it is clear that the eleven "old" ages mark a Proterozoic magmatism and not an excess of argon affecting Jurassic dolerites. This is supported by the fact that: (1) the "old" samples show clearly distinct chemical characteristics; (2) there is no intermediate age between ~180 Ma and the minimum apparent age of 851 Ma displayed by the "old" samples.

The ages obtained during this study indicate that the older part of the swarm was emplaced probably between 900 and 1300 Ma with one plateau and one weighted-mean ages at ~1 Ga. This presumably Mesoproterozoic intrusive event is roughly contemporaneous and shares geochemical features (e.g. low-TiO_2) with the ~1.1 Ga Umkondo large igneous province (e.g. [16]). This LIP covers southern Africa and possibly extended into Antarctica and the Laurentia paleo-continent. Further geochemical investigations (in progress) are

required for a full assessment of the cognate origin of Proterozoic ODS with mafic rocks attributed to the Umkondo igneous province.

In spite of the expedience of the "speedy" experiments compared to classical step heating dating, it represents nevertheless a "time consuming" method if applied to the whole dyke swarm. Therefore, available ages were used to test a valid geochemical discriminant between these two ODS dyke populations, that can be applied to undated samples.

Petrographic features reported above indicate that both Jurassic and Proterozoic dolerite samples share common features (paragenesis dominated by plagioclase, clinopyroxene and magnetite, variable amounts of alteration products in both groups), but they also display some differences. Jurassic rocks are free of amphibole (except the more differentiated rock Bot0089), while this mineral (sometimes associated with biotite) occurs in most of the Proterozoic samples except two sills (Bot11 and Bot0003) and one dyke (Bot0035). Micropegmatite is also commonly (but not always) observed in Proterozoic rocks. Therefore, although petrographic characteristics may partially discriminate these two dyke groups, they remain an ambiguous discriminant.

A geochemical discrimination, based on immobile elements, is therefore required. The plot of age versus TiO_2 content (Fig. 7) discriminates ODS Proterozoic and Jurassic dykes with almost no overlap, the boundary between the two groups being defined by 2.15 wt% TiO_2. ODS Proterozoic dykes display low-Ti and low-P-Zr characteristics whereas Karoo ODS dykes exhibit high-Ti-P-Zr affinity. The discriminant Ti-P-Zr-Mg# relationships established from the dated samples can therefore be applied to assign the 34 undated samples to either the Jurassic or Proterozoic group (Fig. 6). Except the more differentiated rock sample Bot0049 and the low-Ti sample Bot0093, all the undated samples clearly overlap the field of Jurassic dated samples, supporting their Karoo age. Two more evolved rock samples (undated and altered Bot0049 and dated Bot0089) are marked by lower Mg# and higher Zr and P_2O_5 values (Fig. 6) and thus plot out of the main basaltic ODS fractionation trend. For these two samples, TiO_2 content (i.e. the discriminant factor) is shifted towards values lower than expected from the linear Jurassic differentiation trend, so the sample Bot0049 is ambiguously located at the border between low- and high-Ti populations and at the end of the basaltic fractionation trend of low-Ti Proterozoic samples. The magmatic fractionation of Ti-magnetite is responsible for an important TiO_2 decrease for these samples. Although the sample Bot0049 remains undated, it is more likely part of the Jurassic population. Applied to the ODS, our discriminant method remains valid without any ambiguity, provided that the two different-aged populations have tholeiitic basaltic compositions and display relatively low degree of differentiation, i.e. before significant Fe-Ti oxides fractionation. Applied to the whole data set (77 samples), our geochemical discrimination indicates that 90% of the dykes belong to the Jurassic Karoo event, whereas 10% are Proterozoic (the three sills are not included in the counting).

Among 150 dykes observed in the field, 77 fresh dykes were sampled. The unsampled dykes were strongly weathered and possibly predominantly Proterozoic. Thus the real proportion of the Proterozoic dykes in the ODS may be higher than 10%. Nevertheless, because ground magnetic surveys [6] reveal the existence of 423 dykes along the Shashe river section, the above estimation may concern only one-sixth of the whole ODS.

5.3. Geological implications: the role of structural inheritance

Many models were advanced to explain the origin of CFB and their link to continental breakup. These models vary between two end-members: (1) "active" models in which a mantle-plume head is directly responsible for the rifting and associated magmatism by impinging and eroding the lithosphere (e.g. [17]), (2) "passive" models which can be

illustrated by the model of Anderson (e.g. [18],[19]) consisting of a thermal incubation under the mega-continents (shield-effect) with subsequent melting of the perisphere (i.e. enriched upper part of the upper mantle) providing the CFB. More recently, alternative polyvalent models invoke the combination of the above models but with a more important role played by the inherited characteristics of the lithosphere, e.g. beneath ancient orogenic belts [20] or pre-existing lithospheric heterogeneities [21].

Concerning the Karoo igneous province, along with the N-S trending Lebombo and the N70°-oriented Sabie monocline, the giant N110°-trending ODS is one of the three branches of the presumed triple junction (e.g., [2],[17],[22],[24]; Fig. 1). It is usually inferred that this Karoo triple junction system was triggered by the impact of a mantle plume head centered either on the Nuanetsi area ([25,17]), on the lower Zambezi [25] or possibly on the eastern Maputo coast (Mozambique) [26].

The ODS intrudes the Archaean Zimbabwe craton and Limpopo-Shashe orogenic belt and represents an arm of the Karoo triple-junction [17]. The direction of dykes depends on the stress and strain affecting the host rocks during their emplacement, and the geological structures crossed by the dykes. It has been recently proposed on the basis of field geological evidence in this region [27], that dykes emplacement might have been strongly influenced by older structures, whereas Ernst et al. [23] suggest that many large swarms (in other regions of the world) transect a variety of host rock types and tectonic grains with only minor deflections. Proterozoic $^{40}Ar/^{39}Ar$ ages obtained on dykes along the ODS confirm the first hypothesis [27], and indicate that this major N110° tectono-magmatic structure was active during the Proterozoic and was reactivated (acted as a weakened path-trend) during the emplacement of Karoo dykes. Two observations strengthen this proposition, (1) the Proterozoic dykes occur mainly within the central part (Fig. 2a) of the seemingly more extended Jurassic dyke swarm, and (2) the orientation of the investigated Proterozoic and Jurassic dykes is exactly the same (Fig.8). It is therefore unlikely that the orientation of these two diachronic dyke swarms is only the result of similar stress pattern. Therefore, the geometry of the Karoo triple junction is likely not a pristine Jurassic structure directly induced by the impact of a plume head on the lithosphere, as previously proposed, since its most important ODS branch is controlled by a major Proterozoic weak zone.

Although the unquestionable inheritance of the ODS can rule out a pure "active" plume-head model as triggering the "triple junction", it is more speculative, in the state of our knowledge, to discriminate between other models based on structural control. More data are required on the Karoo dyke swarms and particularly on the Sabie-Limpopo and Olifants River Dyke Swarm branches (Fig. 1) (in progress) to get a better idea about the role of pre-existing structures in the Karoo triple-junction. Important to stress is that Marsh pointed out that the NNE-trending Olifants River Dyke Swarm could be older than the Jurassic and possibly includes Precambrian dykes [28].

5.4. Implications for other CFB related dyke swarms.

Continental flood basalts are often associated with giant to medium-size dyke swarms that are used as stress (or/and strain) markers, without ascertaining the eventual role of inheritance in their geometry (although several cases of superposed but genetically unrelated dykes were previously documented).

Concerning Proterozoic CFBs, the Mackenzie dyke swarm (northwestern Canada), the largest radiating dyke swarm on Earth, yielded U-Pb baddeleyite ages of 1267 ± 2 Ma [29,30] and is coeval to the Coppermine flood basalts and the ultramafic Muskox intrusion [1]. This

NW-trending dyke swarm is flanked by a minor and younger NW-trending Franklin dyke swarm dated by U-Pb zircon/baddeleyite at 723 +4/–2 Ma [31]. Although the Franklin dyke swarm flanks the east of the Mackenzie swarm, the parallelism of these two dyke swarms has been controlled by a single crustal weak zone [1].

Buchan et al. [32] reported geographically superposed dyke populations in southern Canada yielding U-Pb baddeleyite ages of 2210 Ma (Senneterre dyke swarm), 2167 Ma (Biscotasing dyke swarm) and 1140 Ma (Abitibi dyke swarm).

Inheritance during the emplacement of radiating or rift triple-junction dyke swarms has never been clearly documented in Phanerozoïc large igneous provinces. These dyke systems should be carefully (re-)investigated to address the following two questions: 1) Is a giant dyke swarm, with a well defined trend, composed of only one or different (as for ODS) generation(s) of dykes?; 2) Is an apparently radiating dyke system (or a triple-junction dyke system) composed of coeval dykes (i.e. related to the same LIP), whatever their trend, or do some trends belong to older dyking periods, making the general pattern misleading?

The first case can apply to the Red Sea rift that is flanked by a 1700 km long coastal gabbroic dyke system emplaced at ca. 24-21 Ma [33] and representing one of the oldest major structural elements of the Red Sea. Most maps of this dyke system [34-37] are confusing because they include Neoproterozoic and Cenozoic dykes displaying the same trend in the northern part of the swarm ([38] and unpublished data). The Proterozoic and Neogene dykes are low-Ti and high-Ti respectively (H.B. and G.F., unpublished data), as for the ODS. A systematic investigation of this composite giant dyke swarm would be therefore required to screen the two dyking episodes and to evaluate the role of structural inheritance during the Red Sea rifting.

This approach could also apply to LIPs such as the Parana-Etendeka characterized by triple-junction dyke swarms, mainly intruding the Precambrian basement. These dyke swarms are related to the Cretaceous Parana LIP, either synchronous or late, compared to the flood basalts (ca. 131 Ma; [39]). However, as the available data concern the freshest samples, the possible presence of older (more altered) dykes and therefore the role of inheritance for some of these three branches have not been tested. The method developed here would allow a systematic investigation of the dykes (including more altered dykes), preventing a possible bias due to the field selection based on the freshness of the samples.

The second case can be illustrated by the early Jurassic central Atlantic magmatic province (CAMP) which is classically interpreted as being related to a radial dyke pattern since the pioneer work of May [41], subsequently used in several papers [1,42,43]. A closer inspection shows that some of these dyke swarms are not CAMP-related, although they fit the radial pattern of May: e.g. in Guyana, Surinam, French Guyana, the investigated NNE-SSW to NE-SW trending dykes are all (but one) Proterozoic (1.4-1.8 Ga by $^{40}Ar/^{39}Ar$ plagioclase and at 1.59-1.64 Ga by Rb/Sr isochron), while the NNW-SSE trending Jurassic CAMP dykes were emplaced at ~200 Ma [40,44-47]. In that case, the two dyke systems also differ chemically, the Proterozoic and Mesozoic dykes being low-Ti and high-Ti mafic rocks respectively [40,48-50]. On the other hand, none of the NE-SW to ENE-WSW trending dykes mapped in Mauritania by May [41] have been dated, and whether they are Proterozoic or Mesozoïc is still unknown.

These examples highlight how the screening of different dyking episodes within the same swarm or within radial dyke patterns could be easily improved using the method developed here, allowing a better evaluation of the role of the structural inheritance during the emplacement of LIPs.

6. Conclusions

Thirty-four new $^{40}Ar/^{39}Ar$ dates and seventy-seven geochemical analyses on the ODS (among 150 dykes sampled) supply crucial new informations on the most prominent dyke swarm of the Karoo triple-junction allowing the following conclusions:

1. The new $^{40}Ar/^{39}Ar$ step-heating plateau and mini plateau ages obtained on the ODS support our preliminary data [4] allowing us to precisely constrain the emplacement of the Karoo dykes between 178.4 ± 1.1 Ma and 180.9 ± 1.3 Ma. The data yield a probability peak at 179 Ma and attest to a short duration of ~2 Ma for the Karoo ODS igneous event. The ODS emplacement was coeval with the outpouring of Karoo lava-flows in NW Zimbabwe defining a northern Karoo igneous sub-province apparently emplaced ~5 Ma after the southern Karoo sub-province (peak at ~184 Ma).
2. $^{40}Ar/^{39}Ar$ dates (thirty-four data, including "speedy" step-heating) show that ODS includes Proterozoic dykes (eight data). Eight dykes and three sills yield imprecise ages between 850-1700 Ma with one plateau age at 958.3 ± 4.6 Ma, and one possibly geologically significant weighted-mean age of 982.7 ± 4.0 Ma.
3. Available radiometric data on the ODS Proterozoic intrusions are not precise enough to assess their exact emplacement age. However, whole population weighted-mean age, (along with one plateau and one possibly significant weighted-mean age) coupled with geochemistry suggest that they could be linked to the ~1.1 Ga Umkondo igneous province. Additional constraints are required to assess this interpretation (work in prep.).
4. The relationship between age and geochemical composition (based on immobile elements, e.g. TiO_2, P_2O_5 and Zr) relationship suggests that ODS includes at least 10% of Proterozoic dykes located in the central part of the Jurassic swarm. The ODS branch of the so-called Nuanetsi triple junction is therefore an inherited Proterozoic structure reactivated during the Jurassic and thus, there is no pristine Jurassic Nuanetsi triple junction mainly hypothesized on the basis of the radiating dyke swarms (ODS being the most prominent of these dyke swarms). This leads us to question whether the Karoo triple junction dyke pattern as being triggered by the arrival of a starting mantle plume head.
5. Therefore, it is desirable to apply the fast age/chemical composition discrimination method developed here to the other presumed Karoo dyke swarms, especially the Olifants River dyke swarm and the Sabi-Limpopo dyke swarm (in progress), in order to better constrain the role of structural inheritance in the whole system of Karoo radiating dyke swarms (i.e. triple junction).
6. Most Phanerozoïc CFB provinces include (giant) dyke swarms in their structure, but it remains unclear if these swarms were emplaced along pre-existing fractures forming passive pathway or if they mark a pristine response to any active mantle upwelling (e.g. starting mantle-plume-head impact).

Acknowledgements.

This work is part of a partnership between the University of Botswana and the French Universities of Nice, Lyon and Brest. We acknowledge the financial support of the CNRS (grant INSU Intérieur de la Terre), the French Ministry of Foreign Affairs, the University of Botswana (Grant RPC Kaapvaal Craton Project R#442), the SU-CRI 2E of the University of Western Brittany and the Universities of Nice and Lyon. We are grateful to C. Tonani, Head

of the Cultural and Scientific Service of the French Embassy in Botswana for his support in developing this program, to the Geological Survey of Botswana (Lobatse) and to C. Byron (Gold Gallery), K. Callum (Tati Mining) and D. Hoffman (BCL Mining) for their field assistance. M. Manetti is thanked for analytical assistance. Géosciences Azur contribution No. 433. We are grateful to R. Ernst and P. Renne for reviews and constructive comments and to C. Wibberley for helpful discussion.

References

[1] R.E. Ernst, J.W. Head, E. Parfitt, E. Grosfils, L. Wilson, Giant radiating dyke swarms on Earth and Venus, Earth Sci. Rev. 39 (1995) 1-58.

[2] R.E. Ernst, K.L. Buchan, Giant radiating dyke swarms: Their use in identifying Pre-Mesozoic Large Igneous Provinces and Mantle Plumes, in: J.J. Mahoney, M.F. Coffin, (Eds.), Large Igneous Provinces: Continental, Oceanic and Planetary Flood Volcanism, Geophysical Monograph 100, American Geophysical Union, Washington, 1997, pp. 297-333.

[3] M. Elburg, Goldberg A., Age and geochemistry of Karoo dolerite dykes from northeast Botswana, J. Af. Earth Sciences 31 (2000) 539-554.

[4] B. Le Gall, G. Tshoso, F. Jourdan, G. Féraud, H. Bertrand, J.J. Tiercelin, A.B. Kampunzu, M.P. Modisi, J. Dyment, M. Maia, $^{40}Ar/^{39}Ar$ geochronology and structural data from the giant Okavango and related mafic dyke swarms, Karoo igneous province, Botswana, Earth Planet. Sci. Lett. 202 (2002) 595-606.

[5] S. Chavez Gomez, A catalogue of dykes from aeromagnetic surveys in eastern and southern Africa, ITC publication number 80, 2001.

[6] G. Tshoso, J. Dyment, C. Aubourg, B. Legall, J.J. Tiercelin, G. Féraud, H. Bertrand, F. Jourdan, A.B. Kampunzu, Magnetic Investigations on the Okavango Giant Dyke Swarm (N Botswana), E.G.S. XXVII, ed. 4, Geophysical Research Abstracts, Nice, 2002, pp. 78

[7] G. Turner, J.C. Huneke, F.A. Podose, G.J. Wasserbrug, $^{40}Ar/^{39}Ar$ ages and cosmic ray exposure agse of Appolo 14 samples, Earth Planet. Sci. Lett. 12 (1971) 19-15.

[8] M.J. Le Bas, R.W. Le Maitre, A. Streickeisen, and B. Zanettin, A chemical classification of volcanic rocks based on the total alkali silica diagram, J. Pet. 27 (1986) 745-750.

[9] K.G. Cox, R. MacDonald, G. Hornung, Geochemical and petrographical provinces in the Karoo basalts of southern Africa, Am. Mineral. 52 (1967) 1451-1474.

[10] R.J. Sweeney, A.R. Duncan, A.J. Erlank, Geochemistry and petrogenesis of Central Lebombo basalts from the Karoo Igneous Province, J. Pet. 35 (1994) 95-125.

[11] D.L. Jones, R.A. Duncan, J.C Briden, D.E Randall, C. MacNiocaill, Age of the Batoka basalts, northern Zimbabwe, and the duration of Karoo Large Igneous Province magmatism, G3 2 (2001) 1-15.

[12] K. Min, R. Mundil, P.R. Renne, K.R. Ludwig, A test for systematic errors in $^{40}Ar/^{39}Ar$ geochronology through comparison with U-Pb analysis of a 1.1 Ga rhyolite, Geochem. Cosmochem. Acta 64 (2000) 73-98.

[13] R.A. Duncan, P.R. Hooper, J. Rehacek, J.S. Marsh, A.R. Duncan, The timing and duration of the Karoo igneous event, southern Gondwana, J. Geophy. Res. 102 (1997) 18127-18138.

[14] J. Encarnacion, T. H., Fleming, H., Elliot, H. V., Eales, Synchronous emplacement of Ferrar and Karoo dolerites and the early breakup of Gondwana, Geology 24 (1996) 535-538.

[15] P.R. Renne, $^{40}Ar/^{39}Ar$ age of plagioclase from Acapulco meteorite and the problem of systematic errors in geochronology, Earth Planet. Sci. Lett. 175 (2000) 13-26.
[16] R.E. Hanson, M.W. Martin, S.A. Bowring, H. Munyanyiwa, U-Pb zircon age for the Umkondo dolerites, eastern Zimbabwe: 1.1 Ga large igneous province in southern Africa-East Antarctica and possible Rodinia correlations, Geology 12 (1998) 1143-1146.
[17] I.H. Campbell, R.W. Griffiths, Implications of mantle plume structure for the evolution of flood basalts, Earth Planet. Sci. Lett. 99 (1990) 79-73.
[18] D.L. Anderson, Y. S. Zhang, T. Tanimoto, Plume heads, continental lithosphere, flood basalts and tomography, in:, B.C. Storey, T. Alabaster, R.J. Pankhurst, (Eds.), Magmatism and the Causes of Continental Break-up, Spec. Pub. Geol. Soc. Lond. 68, 1992, pp. 99-124.
[19] D.L. Anderson, Lithosphere, asthenosphere and perisphere, Reviews of geophysics 33 (1995) 125-149.
[20] A. Tommasi, A. Vauchez, Continental rifting parallel to ancient collisional belts: an effect of the mechanical anisotropy of the lithospheric mantle, Earth Planet. Sci. Lett. 185 (2001) 199-210.
[21] V. Courtillot, C. Jaupart, I. Manighetti, P. Tapponnier, J. Besse, On causal links between flood basalts and continental breakup, Earth Planet. Sci. Lett. 166 (1999) 177-195.
[22] C. Reeves, A failed Gondwana spreading axis in southern Africa, Nature 273 (1978) 222-223.
[23] R.E. Ernst, K.L. Buchan, H.C. Palmer, Giant dyke swarms: characteristics, distribution and geotectonic applications, in: G. Baer, A. Heinmann (Eds.) Physics and chemistry of dykes, Bakema publication, Rotterdam, 1995, pp. 3-21.
[24] D.H. Elliot, T.H., Fleming, Weddell triple junction: The principal focus of Ferrar and Karoo magmatism during initial breakup of Gondwana, Geology 28 (2000) 539-542.
[25] K. Burke, J.F. Dewey, Plume generated triple junctions. Key indicators in applying plate tectonics to old rocks, J. Geol. 81 (1972) 403-433.
[26] K.G. Cox, Karoo igneous activity, and the early stages of the break-up of Gondwanaland, in: B.C. Storey, T. Alabaster, R.J. Pankhurst, (Eds.), Magmatism and the Causes of Continental Break-up, Spec. Pub. Geol. Soc. Lond. 68, 1992, pp. 137-148.
[27] M.K. Watkeys, Development of the Lebombo rifted volcanic margin of southeast Africa, in: M.A. Menzies, S.L. Klemperer, C.J. Ebinger, J. Baker (Eds), Volcanic rifted margins: boulder, Colorado, Geol. Soc. Am. Spec. pap. 362, 2002, pp. 29-48.
[28] J.S. Marsh, Discussion " The geophysical mapping of Mesozoic dyke swarms in southern Africa and their origin in the disruption of Gondwana"., J. Af. Earth Sciences 35 (2002) 525-527.
[29] A.N. Le Cheminant, L.M. Heaman, Mackenzie igneous events, Canada: Middle Proterozoic hotspot magmatism associated with ocean opening, Earth Planet. Sci. Lett. 96 (1989) 38-48.
[30] A.N. Le Cheminant, L.M. Heaman, U-Pb ages for the 1.27 Ga Mackenzie igneous events, Canada: Support for a plume initiation model, Program with Abstracts, Geol. Assoc. Can. 16 (A73), 1991.
[31] L.M. Heaman, A.N. LeCheminant, R.H. Rainbird, Nature and timing of Franklin igneous events, Canada: Implications for a Late Proterozoic mantle plume and the break-up of Laurentia, Earth Planet. Sci. Lett. 109 (1992) 117-131.
[32] K.L. Buchan, J.K. Mortense, K.D. Card, North-east-trending Early Proterozoic dykes of southern Superior Province: multiple episodes of emplacement recognized from

integrated paleomagnetism and U-Pb geochronology, Can. J. Earth Sci. 30 (1993), 1286-1296.
[33] A. Sebai, V. Zumbo, G. Féraud, H. Bertrand, A.G. Hussain, G. Giannérini and R. Campredon, $^{40}Ar/^{39}Ar$ dating of alkaline and tholeiitic magmatism of Saudi Arabia related to the early red Sea rifting, Earth Planet. Sci. Lett. 104 (1991) 473-487.
[34] D.C. Almond, Geological evolution of the Afro-Arabian dome, Tectonophysics 131 (1986) 301-332.
[35] Y. Eyal, M. Eyal,, Mafic dyke swarms in the Arabian-Nubian shield, Israelian Journal of Earth Sciences 36 (1987) 195-211.
[36] M.R. Hempton, Constraints on Arabian plate motion and extensional history of the Red Sea, Tectonics 6 (1987) 687-705.
[37] V.E. Camp, M.J. Roobol, Comment on" Topographic and volcanic asymmetry around the Red Sea: constraints on rift models" by T.H. Dixon, E.R. Ivins and J.F. Brenda, Tectonics 10 (1991) 649-652.
[38] F.B. Davies, Reconnaissance geology of the Duba quadrangle, Sheet 27/35D, Kingdom of Saudi Arabia, Geological map GM-57, Kingdom of Saudi Arabia, Ministry of Petroleum and Mineral Resources, 1980.
[39] P.R. Renne, K. Deckart, M. Ernesto, G. Féraud, E. Piccirillo, Age of the Ponta Grossa dike swarm (Brazil), and implications to Parana flood volcanism, Earth Planet. Sci. Lett. 144 (1996) 199-211.
[40] K. Deckart, G. Féraud, H. Bertrand, Age of Jurassic continental tholeiites of French Guyana, Surinam and Guinea. Implications for the initial opening of the Central Atlantic Ocean, Earth Planet. Sci. Lett. 150 (1997) 205-220.
[41] P.R. May, Patterns of Triassic diabase dikes around the north Atlantic in context of predrift position of the continents, Geol. Soc. Am. Bul. 82 (1971) 1285-1292.
[42] R.I. Hill, Starting plume and continental break-up, Earth Planet. Sci. Lett. 104 (1991) 398-416.
[43] M. Wilson, Thermal evolution of the Central Atlantic margins: continental break-up above a Mesozoic super-plume, J. Geol. Soc. London 154 (1997) 491-495.
[44] H.N.A. Priem, N.A.I.M. Boelrijk, E.H. Hebeda, R.H. Verdurmen, E.A.Th., R.H. Vershure, Isotopic age determination on Surinam rocks, 4. Ages of basement rocks in North-Western Surinam and of the Roraima tuff at Tafelberg, Geol. Mijnbouw 47 (1968) 191-196.
[45] Marzoli, A., P. Renne, E. Piccirillo, M. Ernesto, G. Bellieni, and A. De Min, Extensive 200-million-year-old continental flood basalts of the Central Atlantic Magmatic Province, Science 284 (1999) 616-618,
[46] E.H. Hebeda, N.A.I.M. Boelrijk, H.N.A. Priem, E.A.T. Verdurmen, R.H. Verschure, Excess Radiogenic Argon in the Precambrian Avanavero dolerite in western Suriname (South America), Earth Planet. Sci. Lett. 20 (1973) 189-200.
[47] A. Choudhuri, A.N. Sial, E.P. Oliveira, Unmetamorphosed Proterozoic tholeiite dykes from the northern Amazon craton, Guiana; the evolution of basaltic magmatism, in: A.J. Parker, P.C. Rickwood, D.H. Tucker (Eds.), Mafic dykes and emplacement mechanisms, Balkema, Rotterdam, 1990, pp. 275-283.
[48] D.D. Hawkes, The petrology of Guyana dolerites, Geol. Mag. 4 (1966) 320-335.
[49] A. Choudhuri, Geochemical trends in tholeiite dykes of different ages from Guiana, Chemical geology 22 (1978) 79-85.
[50] S. Nomade, A. Pouclet, Y. Chen, The French Guyana dolerites dykes: geochemical evidence of three populations and new data for the Jurassic Central Atlantic magmatic province, J. Geodyn. 34 (2002) 595-614.

[51] R.H. Steiger, E. Jager, Subcommission on geochronology: convention of the use of decay constants in geo- and cosmochronology, Earth Planet. Sci. Lett. 36 (1977) 359-362.
[52] H.V. Eales, J.S. Marsh, K.G. Cox, The Karoo igneous province: an introduction, in: A.J. Erlank, (Eds.), Petrogenesis of the volcanic rock of the Karoo Province, Geol. Soc. S. Afr. J. Geol. 13, 1984, pp.1-26.
[53] R.M. Key, N. Ayres, the 1998 edition of the National Geological Map of Botswana, J. Af. Earth Sciences 30 (2000) 427-451.
[54] E.C.I. Hammerbeck, R.J. Allcock, 1:4000000 map of geological map of southern Africa, The Geological society of South Africa (1985)

Legend of tables and figures.

Figure 1. Location of the African Karoo CFB and questionably related dyke swarms (modified after [5,52,53,54]). ODS: Okavango dyke swarm (this study); ORDS: Olifants River dyke swarm (undated; intruding basement); SBDS: South Botswana dyke swarm (undated; intruding Karoo formations); SLDS: Sabi-Limpopo dyke swarm (mostly undated; intruding basement and Karoo formations); SleDS: South Lesotho dyke swarm (undated; intruding Karoo lava-pile) ; SMDS: South Malawi dyke swarm (undated; intruding basement and Karoo group); RRDS: Rooi Rand dyke swarm (undated, intruding Karoo lava-pile); NLDS: north Lebombo dyke swarm (undated, intruding Karoo lava-pile); GDS: Gap dyke swarm (undated, intruding Karoo sediments). Dotted line corresponds to Botswana border. Note that Botswana and western Zimbabwe are mostly covered by desert sand and that the Karoo volcanic rocks are therefore extrapolated from scarce outcrops, boreholes and (aero)magnetic data [5,53].

Figure 2. a) 100 km-long section along the Shashe River, with location of step-heating dated dykes and sills. "Speedy" and conventional step-heating dated Proterozoic intrusives are indicated by (*). Note that dated Proterozoic dykes are clustered near the center of the swarm. b) Sketch map of northeastern Botswana showing the N110° oriented ODS and location of samples along the 150 km-wide main part of the ODS. Lava flows exposures are also indicated. Modified after [4]. The Jurassic "speedy" step-heating ages are not located on this map, but note that they are homogenously distributed along the whole Shashe River section.

Figure 3. $^{40}Ar/^{39}Ar$ and $^{37}Ca/^{39}K$ ratio spectra from ODS plagioclase separates. a) Jurassic and Proterozoic "speedy" step-heating spectra. b) Jurassic and Proterozoic plateau (P), mini-plateau (MP) and weighted-mean (W) age spectra. Ages are given at the 2 sigma confidence level.

Figure 4. age-probability density distribution diagram of twelve $^{40}Ar/^{39}Ar$ plateau / mini-plateau ages compiled from this study and [4] (solid line), seventeen "speedy" step-heating ages (dotted line), twelve integrated ages (i.e. equivalent to K/Ar) from ODS samples which yield plateau ages (from [4] and this study; dashed line) and twelve Ar/Ar plagioclase plateau ages and U/Pb single zircon and baddeleyite ages on Zimbabwe [11] and southern Karoo [13,14]), respectively. Each datum is represented as a unit weight. All data are represented by a gaussian distribution with variance equal to the analytical uncertainties.

Figure 5. Total Alkali-SiO_2 classification diagram [8] of Jurassic (pale grey circles) and Proterozoic (full black circles) ODS samples.

Figure 6. TiO_2, SiO_2 and Zr vs. Mg# [100*Mg/(Mg+Fe^{2+}) with Fe_2O_3/FeO normalized at 0.15] and P_2O_5 vs. TiO_2 variation diagrams for Jurassic (pale grey circles), Proterozoic (black circles) and undated (diamonds) samples of the ODS. Major elements are in wt% and trace elements in ppm.

Figure 7. $^{40}Ar/^{39}Ar$ age (Ma) vs. TiO_2 (wt%) content of Jurassic (plateau / second step ages; pale grey circles) and Proterozoic (integrated age; black circles) ODS samples. Low-Ti / high-Ti discrimination boundary is located at 2.15 wt% TiO_2.

Figure 8. Statistical distribution of direction of Proterozoic (black portions, n=8) and Jurassic (grey portions, n=23) dated dykes (rose diagram). Angular values of each portion represent 6° classes. Length of one portion is proportional to the number of dykes oriented in the same strike direction. Note that the predominant N110° direction includes 70 % of the whole dated dykes population (i.e. Proterozoic and Jurassic)

Table 1.Geographic position (GPS projection: WGS-84), trend and $^{40}Ar/^{39}Ar$ ages of ODS. (a) "Speedy" step-heating experiments on Karoo samples. Both integrated and high temperature ages (excluding pre-degassing step) are given. (b) Classical $^{40}Ar/^{39}Ar$ step-heating dating on Karoo samples. Inverse isochron ($^{36}Ar/^{40}Ar$ vs. $^{39}Ar/^{40}Ar$) ages, initial $^{40}Ar/^{36}Ar$ ratio and mean square weighted deviation (MSWD) are indicated. (c) Both "speedy" and classical step heating experiments on Proterozoic samples. Isochrons for classical step-heating are not reported because steps are too clustered to give reliable value. Analytical uncertainties on the ages are quoted at 2 sigma (2σ) confidence level. * correspond to plateau ages. Both laser (l) and furnace (f) dating were performed on the Proterozoic sample Bot0003. For Bot0048, the orientation is deduced from field observation as no contact was observed but note that the possibility that this intrusion is a sill, remains.

Table 2. (BACKGROUND DATA SET) Detailed plagioclase $^{40}Ar/^{39}Ar$ data from ODS samples. ^{40}Ar*= radiogenic Ar; ^{37}Ar and ^{39}Ar produced by neutron interference with Ca and K respectively. Decay constants are from [51]. Correction factors for interfering isotopes were $(^{39}Ar/^{37}Ar)_{Ca}$ = $7.30x10^{-4}$ (± 4%), $(^{36}Ar/^{37}Ar)_{Ca}$ = $2.82x10^{-4}$ (± 1%) and $(^{40}Ar/^{39}Ar)_K$ = $2.97x10^{-2}$ (± 3%). Analytical uncertainties are quoted at 1 sigma confidence level.

Table 3. (BACKGROUND DATA SET) Major (oxide wt.%) and trace (ppm) elements compositions of fifty-six Jurassic and ten Proterozoic samples from the Okavango dyke swarm. Mg# = [100*Mg/(Mg+Fe^{2+}) with Fe_2O_3/FeO normalized to 0.15]. (s) indicates sills.

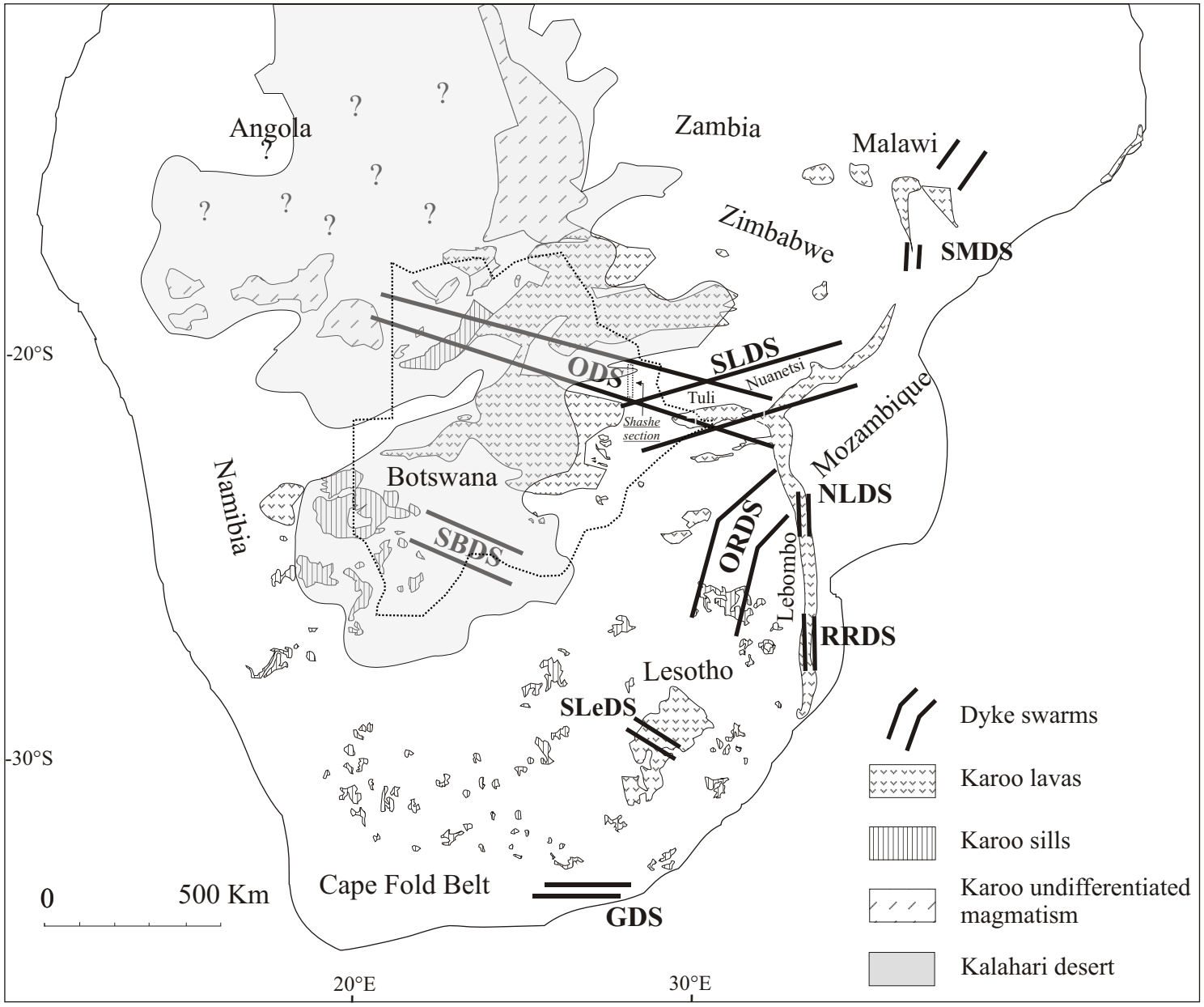

Fig. 1 (Jourdan et al.)

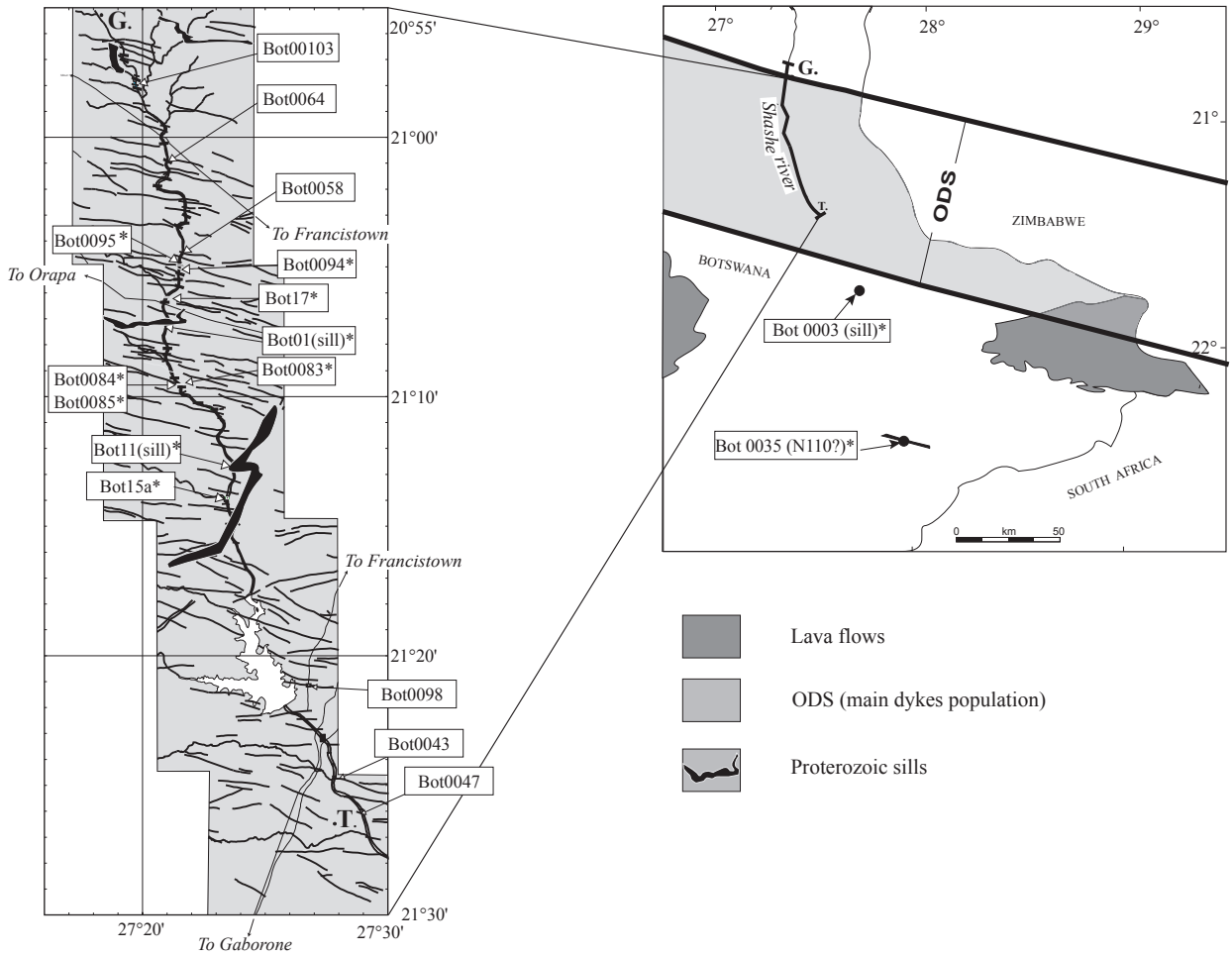

Fig. 2 (Jourdan et al.)

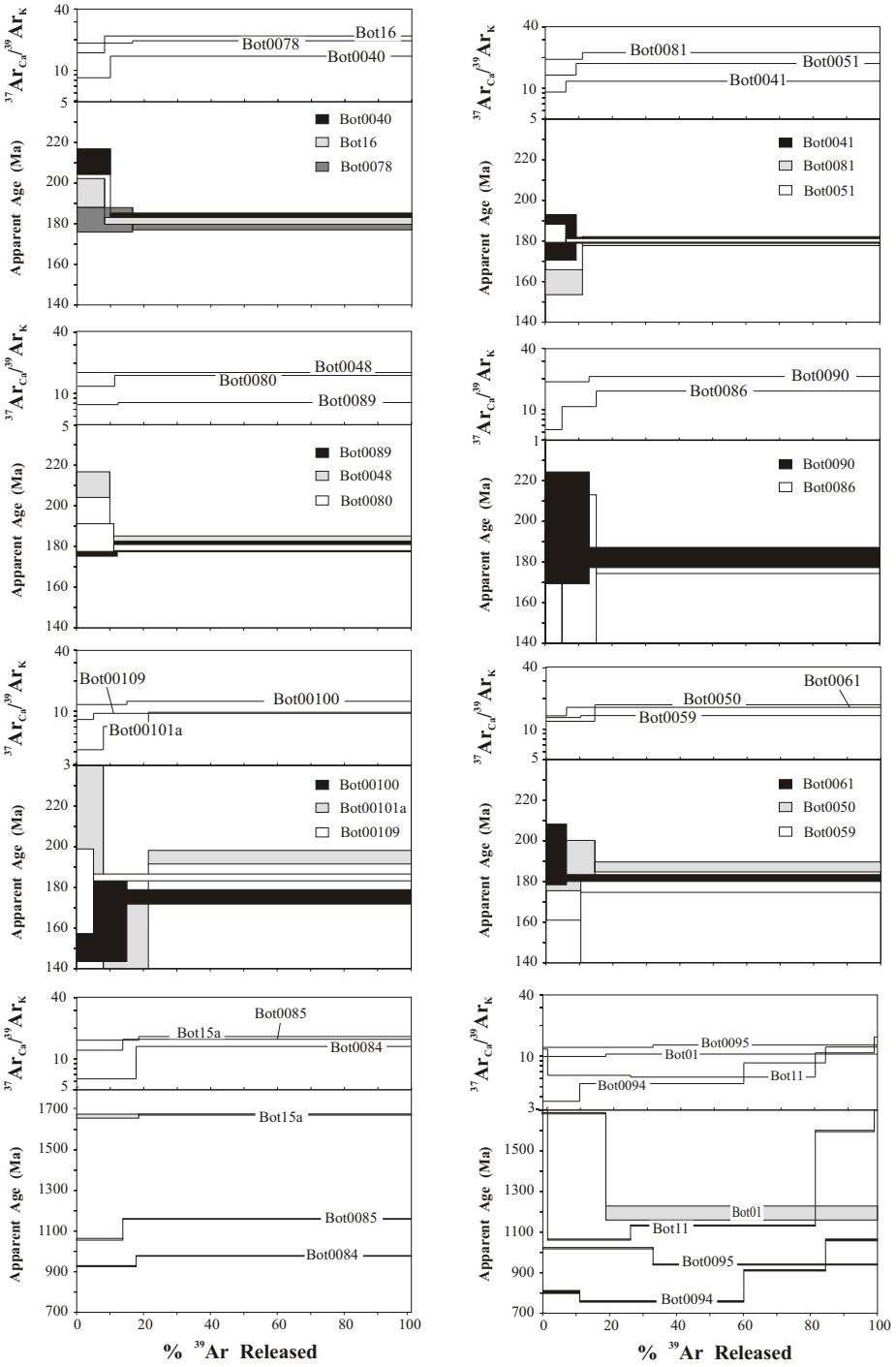

Fig. 3a (Jourdan et al.)

Fig. 3b (Jourdan et al.)

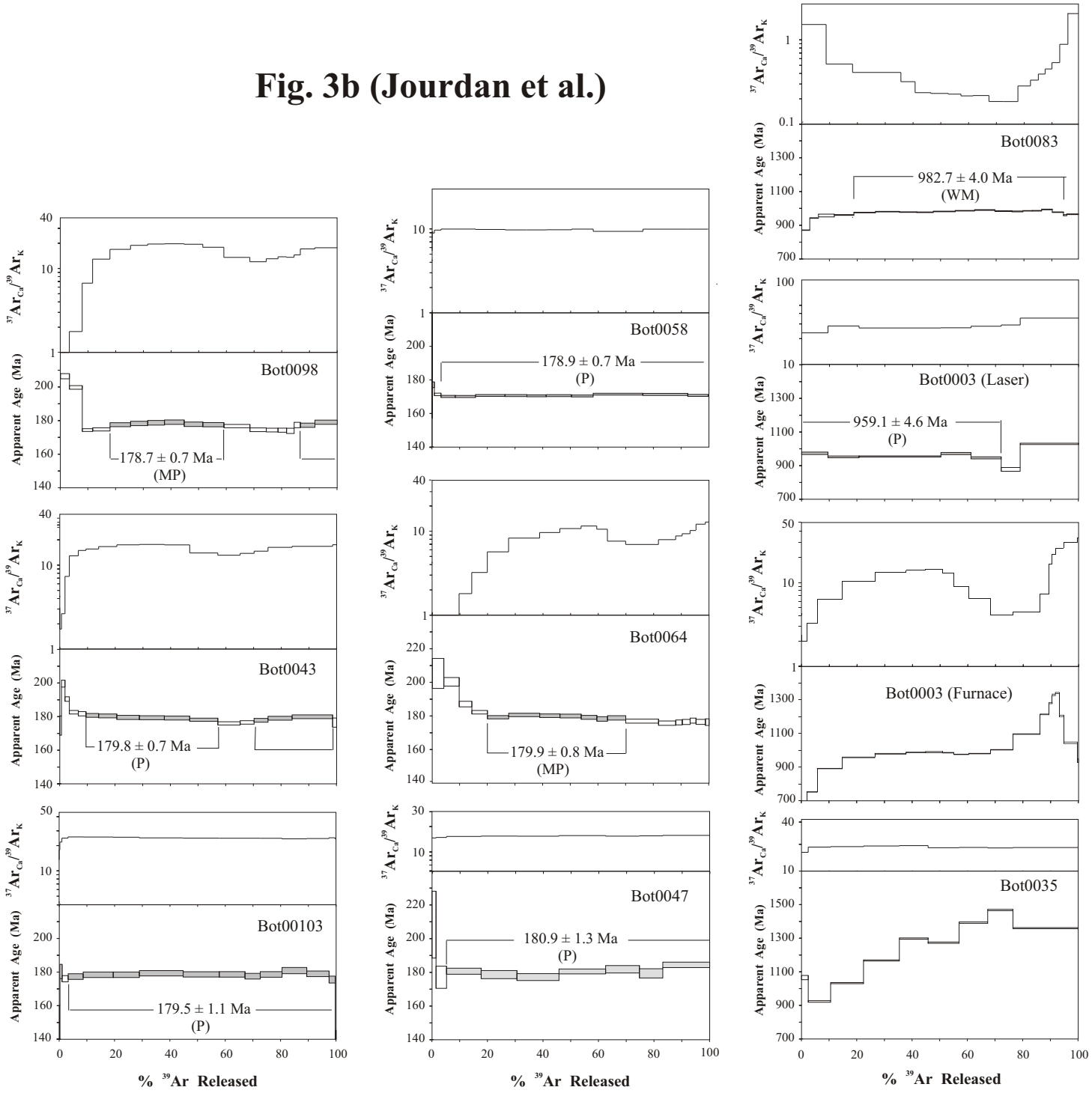

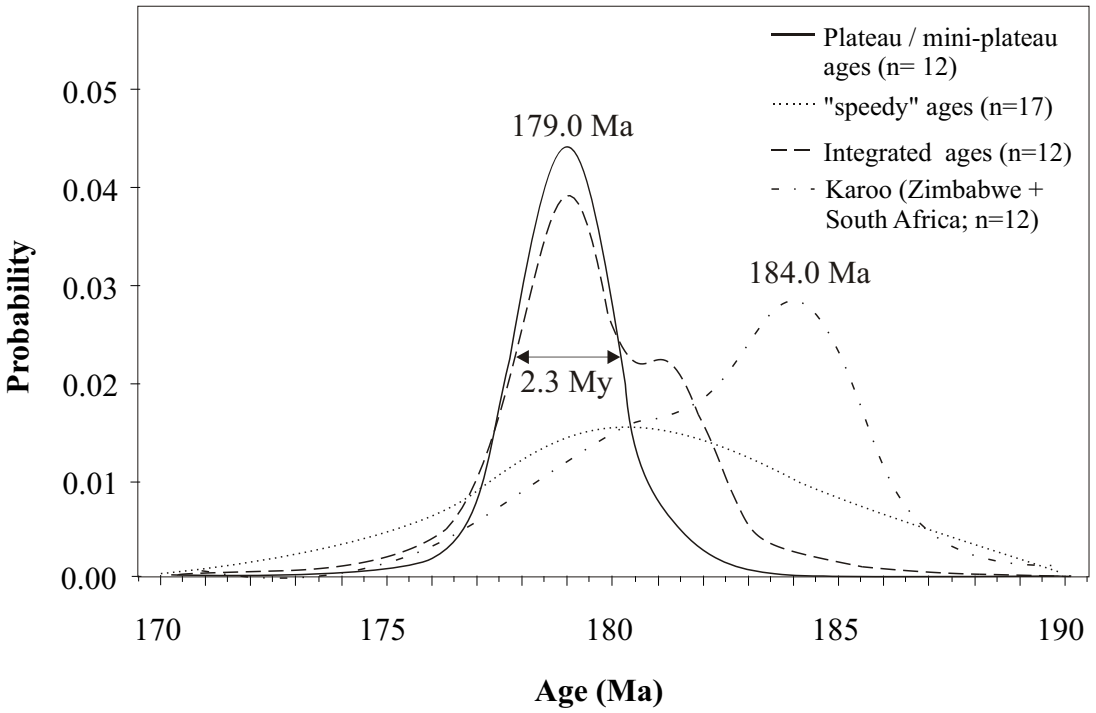

Fig. 4 (Jourdan et al.)

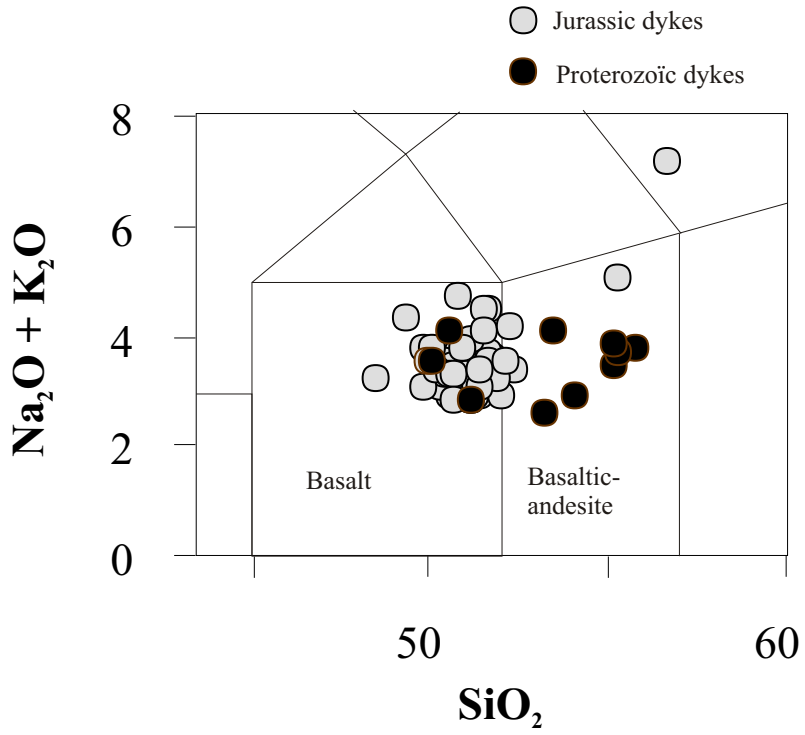

Fig. 5 (Jourdan et al.)

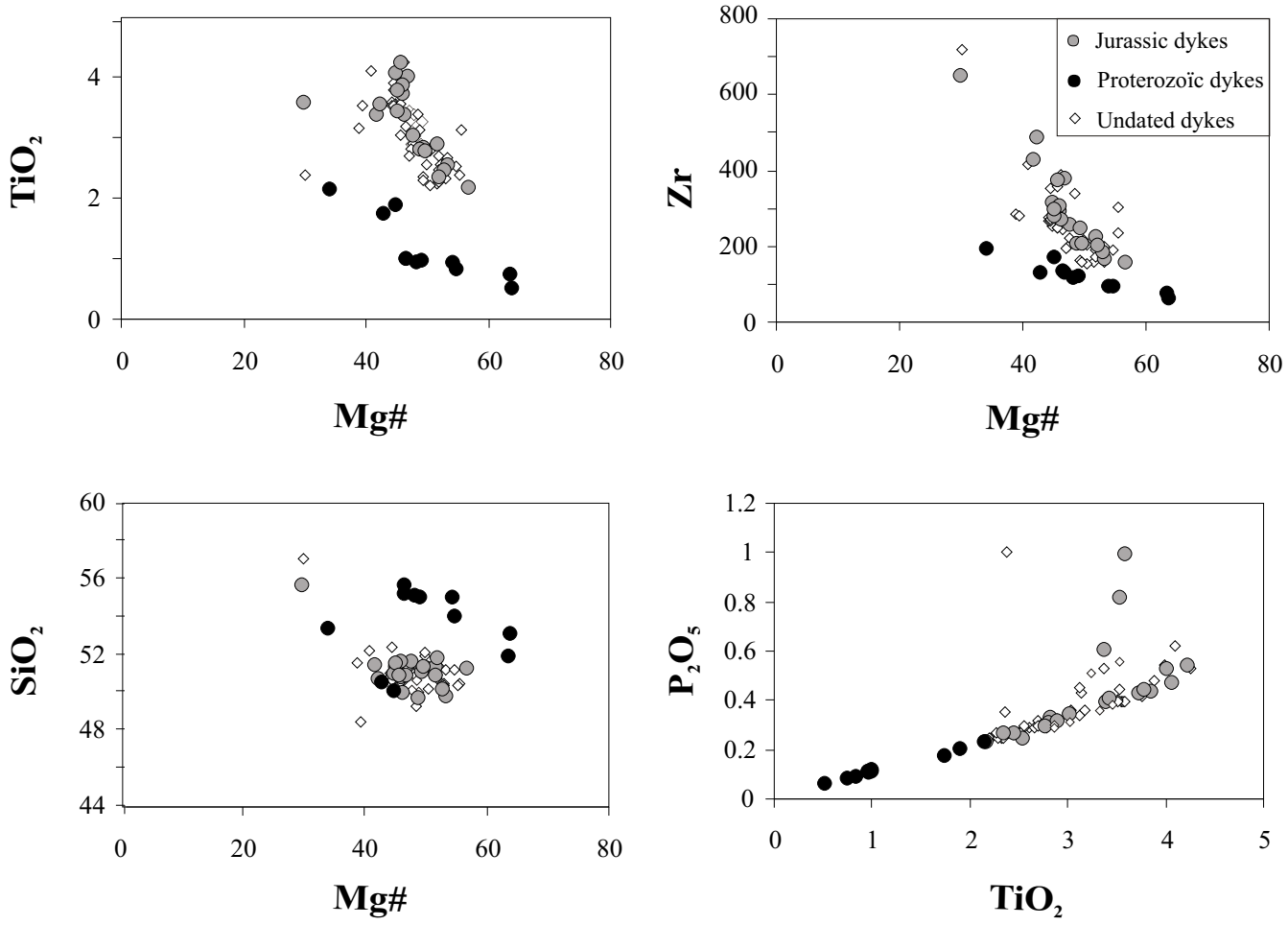

Fig. 6 (Jourdan et al.)

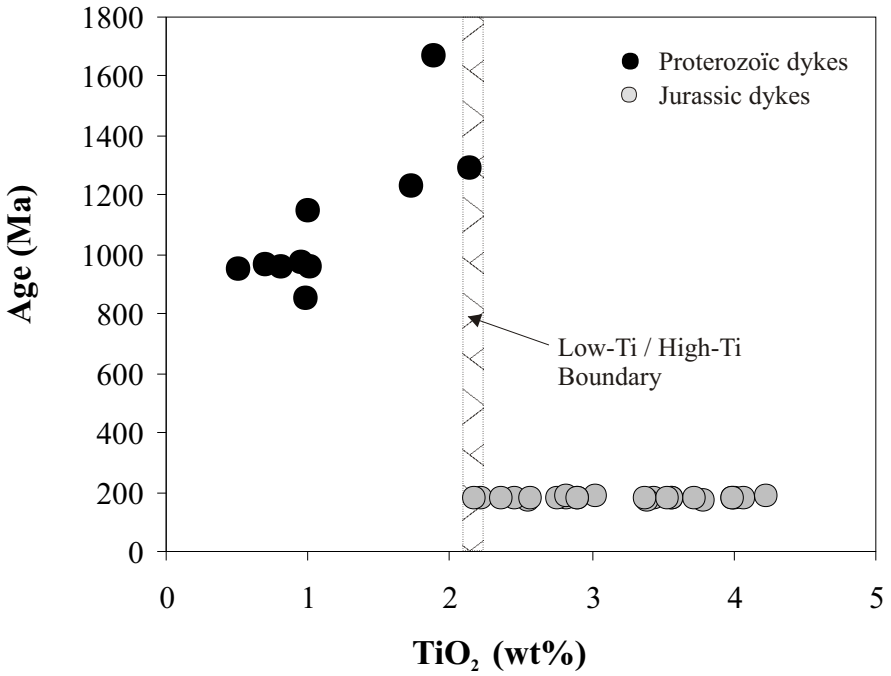

Fig. 7 (Jourdan et al.)

Fig. 8

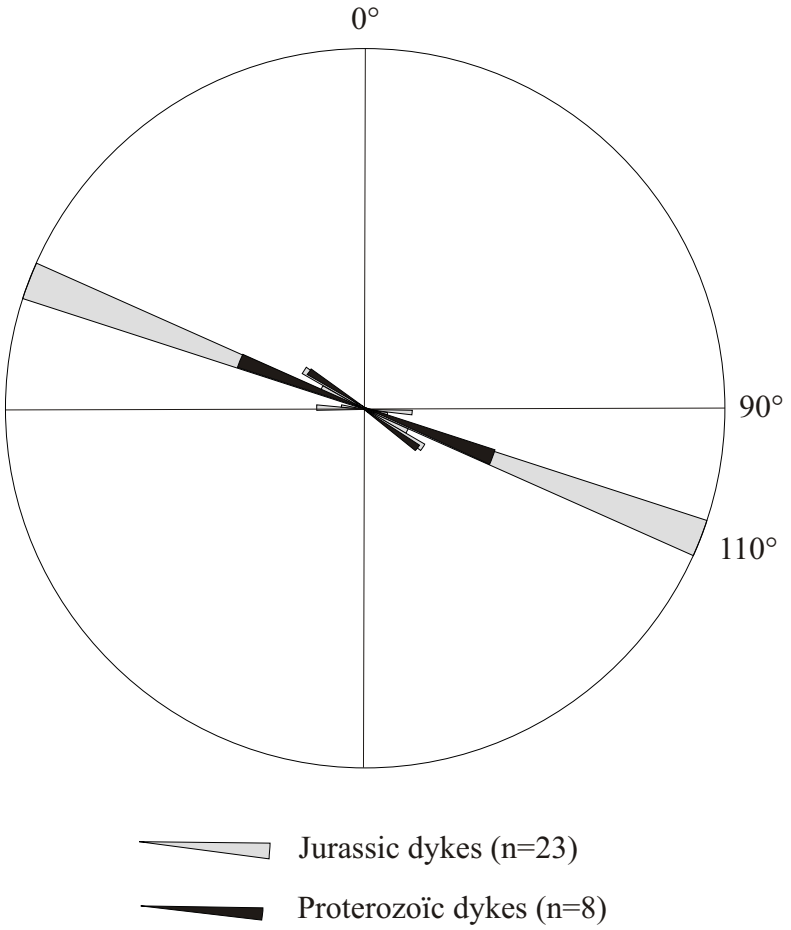

Fig. 8 (Jourdan et al.)

Table 1

(A)

Sample	GPS Coordinates	Dyke orientation	High temperature step age (Ma, ±2s)	Step number	Total ^{39}Ar released (%)	Integrated age (Ma, ±2s)
	ODS in Shashe River (Jurassic)					
bot 16	21°17.514'S 27°21.320'E	N110?	181.4±3.2	fuse	91.8	*182.5± 3.2*
bot0089	21°08.883'S 27°20.469'E	N110	180.4±5.8	fuse	87.8	*180.2±5.2*
bot0078	21°11.375'S 27°23.000'E	N110	178.9±4.0	fuse	83.4	*179.4±3..8*
bot0040	21°24.416'S 27°27.079'E	N110?	184.0±2.6	fuse	90.1	*186.6±2.6*
bot0048	21°26.702'S 27°28.559'E	N120 / sill?	181.1±2.6	fuse	91.8	*180.5±2.6*
bot0080	21°10.620'S 27°21.623'E	N110	179.9±4.4	fuse	88.9	*177.7±3.0*
bot0051	21°27.862'S 27°29.181'E	N90	180.3±3.0	fuse	90.8	*180.5±3.4*
bot00100	20°56.730'S 27°18.784'E	N110	175.4±7.0	fuse	85.0	*173.6±8.5*
bot00109	21°15.084'S 22°22.945'E	N110	184.9±3.4	fuse	95.0	*184.6±3.8*
bot0081	21°10.128'S 27°21.162'E	N120	179.6±3.0	fuse	88.9	*180.1±4.2*
bot0041	21°24.655'S 27°27.272'E	N110	180.3±1.8	fuse	93.8	*180.5±1.7*
bot0061	21°03.211'S 27°21.491'E	N90/110	181.7±3.2	fuse	93.9	*182.4±3.6*
bot0050	21°27.288'S 27°28.681'E	N110?	187.2±5.0	fuse	85.4	*187.3±5.5*
bot0086	21°09.438'S 27°20.551'E	N110	178.3±11.2	2-fuse	84.8	*173.8±16.6*
bot00101a	20°56.667'S 27°18.832'E	N110	194.9±6.6	2-fuse	78.5	*191.5±8.4*
bot0059	21°02.958'S 27°21.484'E	N90	178.8±8.2	fuse	89.6	*175.6±10.0*
bot0090	21°08.883'S 27°20.469'E	N115	182.3±10.0	fuse	86.9	*184.2±11.3*

Table 1

(B)

Sample	GPS Coordinates	Direction	plateau*/ mini-plateau age (Ma, ±2s)	Total ^{39}Ar released (%)	Isochron age (Ma, ±2s)	Steps (°c)/ steps n°	^{40}Ar/^{36}Ar intercept (±1s)	MSWD	Integrated age (Ma, ±2s)
ODS in Shashe River (plateau/mini-plateau ages)									
bot0043	21°25.427'S 27°27.095'E	N120	179.8±0.7*	76.0	180.5±1.7	880-1100; 1350-1500	256.4±29	4.6	*179.9±0.4*
bot0058	21°02.958'S 27°21.484'E	N115	178.9±0.7*	96.5	178.7±1.1	850-1550	297.5±4.5	2.3	*178.9±0.4*
bot0064	20°59.880'S 27°20.433'E	N110	179.9±0.8	50	181.8±2.0	800-1070	233.4±27.7	0.7	*181.5±1.0*
bot0047	21°26.262'S 27°28.530'E	N110	180.9±1.3*	94.8	180.2±7.8	3-8	317.0±86.9	2.5	*181.2±1.4*
bot0098	21°21.720'S 27°26.346'E	N110	178.7±0.7	54.4	178.8±1.2	840-1050; 1400-1600	289.4±5.3	1.9	*179.4±0.4*
bot00103	20°58.002'S 27°19.419'E	N110	179.5±1.1*	96.5	178.9±1.1	800-1550	300.4±41.4	1.9	*179.0±0.5*

(C)

Sample	GPS Coordinates	Direction	Plateau*/ Interpreted age (Ma, ±2s)	Step number	Total ^{39}Ar released (%)	Integrated age (Ma, ±2s)
ODS in Shashe River (Proterozoic)						
bot11	21°13.080'S 27°23.783'E	Sill	-	-	-	*1233.0±4.0*
bot0094	21°02.546'S 27°20.583'E	N110	-	-	-	*851.1±6.0*
bot0095	21°02.546'S 27°20.849'E	N110	-	-	-	*972.0±4.0*
bot15a	21°14.071'S 27°23.573'E	N130	-	-	-	*1672.0±6.0*
bot0084	21°10.044'S 27°21.155'E	N110	-	-	-	*967.4±4.0*
bot0085	21°10.044'S 27°21.155'E	N110	-	-	-	*1146.5±4.0*
bot01	21°07.334'S 27°20.431'E	boulders (sill)	-	-	-	*1297.0±52.0*
bot 17[(1)]	21°06.512'S 27°20.708'E	N110	-	-	-	*951.6±5.0*
bot0083	21°10.044'S 27°21.155'E	N110	982.7±1.0	5 to 17	75.7	*963.3±2.9*
ODS eastern Botswana (Proterozoic)						
bot0003	21°54.903'S 28°02.471'E	Sill	959.1±4.6 (l)*	1 to 5	72.1	*969.1±3.8*
			- (f)	-	-	*999.1±3.8*
bot0035	22°25.283'S 28°15.550'E	N110?	1224.4±10	2	8.0	*1558.5±2.8*

Table 2

	Temperature (°C)/ step n°	Atmospheric contamination (%)	^{39}Ar (%)	$^{37}Ar_{Ca}/^{39}Ar_{K}$	$^{40}Ar^{*}/^{39}Ar$	Age (Ma)		
bot11	1	4.4	1.4	11.7	119.7	1894.5	±	34.7
	2	3.0	24.8	6.5	51.7	1063.0	±	2.8
	3	1.0	55.2	6.2	56.3	1132.3	±	2.6
	4	0.6	17.6	10.8	91.7	1597.1	±	3.2
	fuse	0.0	1.0	15.4	151.8	2184.1	±	53.3
					I.A.=	1233.0	±	2.0
bot0094	1	7.0	11.1	3.6	36.2	804.9	±	7.1
	2	2.3	49.0	5.4	33.6	758.2	±	3.3
	3	1.4	24.4	8.6	42.3	911.3	±	3.0
	fuse	1.6	15.5	12.3	51.5	1061.1	±	4.6
					I.A.=	851.1	±	3.0
bot0095	1	5.0	33.0	12.2	49.4	1020.4	±	3.5
	fuse	1.9	67.0	12.8	44.4	940.1	±	2.5
					I.A.=	972.0	±	2.0
bot15a	1	2.3	18.6	15.3	98.0	1665.4	±	10.0
	fuse	0.9	81.5	16.6	98.7	1673.5	±	3.1
					I.A.=	1672.0	±	3.0
bot0085	1	7.7	17.8	6.4	42.9	927.6	±	2.7
	fuse	1.7	82.2	13.2	45.9	977.7	±	1.6
					I.A.=	967.4	±	2.0
bot0084	1	5.3	13.8	12.2	51.4	1059.5	±	4.4
	fuse	1.6	86.2	15.6	58.0	1160.0	±	1.8
					I.A.=	1146.5	±	1.0
bot01	1	3.9	18.9	9.9	99.9	1684.4	±	3.0
	fuse	5.4	81.1	10.5	60.7	1193.6	±	34.6
					I.A.=	1297.0	±	26.0
bot0083	1	4.3	8.8	1.5	38.2	871.3	±	1.5
	2	0.3	9.5	0.5	42.3	942.8	±	1.6
	3	0.0	17.4	0.4	43.2	958.2	±	8.2
	4	0.2	5.1	0.3	43.3	961.1	±	2.2
	5	0.2	5.7	0.2	44.2	975.8	±	1.7
	6	0.1	6.3	0.2	44.5	981.0	±	1.6
	7	0.2	4.6	0.2	44.4	978.3	±	1.6
	8	0.3	4.3	0.2	44.3	977.2	±	1.8
	9	0.2	5.7	0.2	44.6	981.8	±	1.8
	10	0.3	5.1	0.2	44.8	986.4	±	1.6
	11	0.1	5.3	0.2	45.1	990.7	±	2.0
	12	0.2	4.5	0.3	44.7	984.1	±	1.6
	13	0.3	2.8	0.3	44.6	982.2	±	2.5
	14	0.0	2.4	0.4	44.8	986.0	±	1.6
	15	0.3	2.5	0.5	44.8	986.1	±	2.0
	16	0.1	2.8	0.5	45.3	993.7	±	1.9
	17	0.1	2.9	0.9	44.3	977.7	±	1.5
	18	1.5	0.8	2.1	43.3	960.1	±	3.3
	fuse	0.6	3.4	1.9	43.6	965.8	±	2.2
					I.A.=	963.3	±	1.5
bot0003 (l)	1	12.2	9.5	23.5	46.8	974.3	±	7.0
	2	1.8	11.2	28.3	45.4	953.0	±	5.2
	3	1.9	29.6	26.8	45.6	955.7	±	3.2
	4	2.5	10.9	27.0	46.7	973.0	±	6.4
	5	5.4	10.9	28.1	45.1	947.6	±	6.1
	6	5.8	6.9	29.1	41.0	878.7	±	11.2
	fuse	2.7	21.1	35.2	50.3	1031.0	±	3.6
					I.A.=	969.1	±	1.9

	Temperature (°C)	Atmospheric contamination (%)	^{39}Ar (%)	$^{37}Ar_{Ca}/^{39}Ar_{K}$	$^{40}Ar^{*}/^{39}Ar$	Age (Ma)		
bot0003 (f)	550	90.3	0.1	2.4	13.6	335.6	±	91.6
	650	39.5	1.9	2.0	27.7	629.9	±	3.4
	700	6.9	3.8	3.3	34.4	753.4	±	1.9
	750	3.8	9.1	6.3	42.4	892.2	±	1.4
	790	0.8	11.7	10.2	46.5	958.8	±	2.1
	830	0.4	11.3	13.2	47.8	980.4	±	2.2
	860	0.5	7.0	14.0	48.4	988.7	±	1.7
	890	0.7	6.1	14.3	48.5	990.3	±	3.5
	905	0.6	4.1	13.1	48.2	986.6	±	1.8
	935	1.0	5.4	9.0	47.6	976.5	±	1.5
	960	1.1	7.9	6.5	47.9	981.0	±	1.7
	1030	1.5	8.1	4.1	49.3	1003.8	±	1.7
	1050	1.9	9.9	4.5	55.5	1096.9	±	2.1
	1100	2.6	3.2	7.4	63.7	1214.5	±	2.1
	1150	4.4	1.2	16.5	68.6	1282.0	±	3.8
	1200	5.0	1.1	21.7	72.3	1331.0	±	4.4
	1250	5.1	1.4	25.3	73.2	1342.1	±	3.6
	1300	5.6	1.6	25.5	63.1	1206.1	±	4.4
	1400	5.8	4.9	30.0	52.1	1046.3	±	4.4
	1600	17.4	0.4	33.7	45.3	939.9	±	10.5
					I.A.=	999.6	±	0.6
bot0035	1	13.3	2.4	16.1	73.9	1365.8	±	12.8
	2	2.2	8.1	18.5	63.4	1223.8	±	5.0
	3	1.3	11.9	18.7	71.4	1332.7	±	3.2
	4	0.9	13.0	19.1	82.0	1467.7	±	3.2
	5	0.8	10.4	19.3	93.1	1598.3	±	3.6
	6	0.9	11.2	18.2	90.9	1573.7	±	3.9
	7	0.7	10.3	18.3	101.6	1693.0	±	4.2
	8	0.6	9.1	18.1	108.7	1768.2	±	4.3
	fuse	0.4	23.6	18.3	98.6	1660.0	±	3.5
					I.A.=	1558.5	±	1.4

Table 2

	Temperature (°C) /step n°	Atmospheric contamination (%)	^{39}Ar (%)	$^{37}Ar_{Ca}/^{39}Ar_{K}$	$^{40}Ar^{*}/^{39}Ar$	Age (Ma)		
Bot0043	550	77.2	0.0	3.1	80.1	1439.6	±	375.0
	650	75.3	0.6	1.7	6.7	174.7	±	5.7
	700	19.6	1.3	2.6	7.7	199.7	±	2.0
	750	10.9	1.6	7.3	7.3	190.7	±	1.3
	800	7.1	3.2	12.9	7.0	183.0	±	0.7
	840	3.9	2.8	15.0	7.0	182.1	±	0.9
	880	5.4	4.6	15.6	6.9	181.2	±	0.7
	920	3.7	6.6	16.6	6.9	180.9	±	0.6
	960	2.2	8.2	17.5	6.9	180.0	±	0.7
	1000	1.3	9.0	17.7	6.9	179.8	±	0.6
	1050	2.1	9.2	17.4	6.9	179.7	±	0.6
	1100	6.1	10.2	14.0	6.8	178.5	±	0.5
	1200	8.0	8.1	13.1	6.7	176.3	±	0.6
	1250	7.9	5.1	13.8	6.8	176.9	±	0.6
	1350	5.7	5.0	14.7	6.8	178.2	±	0.8
	1400	3.7	8.7	16.3	6.9	179.5	±	0.6
	1500	3.3	14.6	16.8	6.9	180.4	±	0.5
	1600	3.9	1.5	17.5	6.8	176.9	±	2.5
					I.A.=	179.9	±	0.4
bot0058	550	102.9	0.0	5.5	-	-	±	-
	650	93.8	0.1	8.0	7.8	201.2	±	39.6
	700	57.8	0.2	9.2	8.0	208.0	±	10.8
	750	19.6	0.6	8.9	7.2	186.7	±	2.1
	800	5.1	2.4	9.7	6.9	179.5	±	0.8
	850	2.9	5.1	10.0	6.8	178.0	±	0.5
	900	2.4	7.3	9.9	6.8	178.0	±	0.5
	950	1.7	10.7	9.8	6.8	178.7	±	0.4
	1000	1.5	7.9	9.7	6.8	178.7	±	0.5
	1050	1.3	7.0	9.7	6.8	178.5	±	0.4
	1100	1.2	9.2	9.8	6.8	178.6	±	0.5
	1200	1.6	7.8	9.9	6.8	178.4	±	0.4
	1350	1.3	17.9	9.3	6.9	179.7	±	0.4
	1450	1.0	16.3	9.9	6.9	179.5	±	0.5
	1550	1.1	7.3	9.9	6.8	178.8	±	0.5
	1600	22.0	0.3	9.8	5.4	143.4	±	3.1
					I.A.=	178.9	±	0.4
bot0064	550	100.4	0.1	1.1	-	-	±	-
	650	72.9	4.2	0.6	8.0	205.3	±	8.9
	750	37.2	5.5	0.8	7.8	200.4	±	2.5
	770	22.8	4.6	1.8	7.2	187.2	±	1.6
	780	9.4	5.6	3.2	7.0	182.3	±	1.0
	800	5.5	7.7	5.7	6.9	179.4	±	0.9
	850	4.8	11.2	8.3	7.0	180.9	±	0.9
	880	4.2	7.3	9.6	7.0	180.4	±	0.9
	920	4.2	7.7	10.8	7.0	180.3	±	0.9
	960	4.6	5.7	11.5	6.9	179.5	±	1.0
	1030	8.6	3.8	10.6	6.9	178.5	±	1.2
	1070	15.0	6.6	7.6	6.9	179.1	±	1.2
	1150	13.4	11.8	7.0	6.8	177.1	±	1.1
	1200	14.8	6.2	7.9	6.8	176.0	±	1.2
	1250	15.2	2.3	8.8	6.8	176.4	±	1.4
	1300	15.2	2.8	9.3	6.8	176.7	±	1.4
	1350	13.4	2.1	10.2	6.8	177.5	±	1.4
	1400	14.1	3.4	12.0	6.8	176.9	±	1.3
	1600	17.9	1.3	12.7	6.8	176.8	±	1.8
					I.A.=	181.5	±	0.5

	Temperature (°C)	Atmospheric contamination (%)	^{39}Ar (%)	^{37}ArCa/^{39}ArK	^{40}Ar*/^{39}Ar	Age (Ma)		
bot0098	550	93.4	0.1	1.2	4.9	130.2	±	38.0
	650	52.3	3.2	0.9	8.0	206.5	±	1.5
	700	20.0	4.7	1.8	7.7	199.8	±	1.1
	750	17.1	3.8	6.7	6.7	174.5	±	0.7
	800	11.1	6.3	12.9	6.7	175.1	±	0.6
	840	6.8	7.4	16.9	6.8	178.0	±	0.7
	880	6.2	6.2	18.9	6.9	178.8	±	0.7
	920	5.7	6.1	19.5	6.9	179.2	±	0.8
	960	5.4	7.1	19.7	6.9	179.6	±	0.7
	1000	6.7	6.8	19.4	6.9	178.4	±	0.7
	1050	10.6	7.6	17.9	6.8	178.0	±	0.7
	1100	19.6	9.4	13.6	6.8	177.1	±	0.6
	1150	24.7	5.9	12.0	6.7	174.9	±	0.9
	1200	25.5	4.3	13.0	6.7	174.7	±	0.8
	1250	27.0	3.1	13.8	6.7	174.7	±	0.9
	1300	33.4	2.8	13.6	6.7	174.3	±	1.3
	1350	27.8	2.3	14.5	6.8	177.8	±	1.4
	1400	18.3	5.2	17.1	6.8	177.7	±	0.8
	1600	20.7	8.0	17.7	6.9	179.5	±	0.7
					I.A.=	179.4	±	0.4
bot00103	550	100.4	0.0	13.6	-	-	±	-
	650	94.7	0.2	17.8	5.0	132.2	±	28.4
	700	57.3	0.7	22.1	6.9	181.0	±	4.0
	750	23.0	2.2	24.5	6.8	176.7	±	1.2
	800	10.5	5.4	25.4	6.8	178.0	±	0.8
	850	6.4	10.9	25.3	6.9	179.1	±	0.8
	900	4.0	9.5	25.2	6.9	179.1	±	0.8
	950	2.9	15.8	24.8	6.9	180.0	±	0.7
	1000	2.9	13.1	24.6	6.9	179.3	±	0.7
	1050	2.7	9.3	24.5	6.9	179.3	±	0.8
	1100	6.5	5.5	24.5	6.8	178.2	±	0.9
	1200	14.3	7.9	24.5	6.9	179.3	±	0.9
	1350	31.5	8.9	24.1	7.0	181.5	±	1.2
	1450	25.0	8.1	24.3	6.9	179.6	±	0.9
	1550	19.9	2.2	24.8	6.8	176.2	±	1.5
	1600	44.5	0.3	24.1	5.2	137.2	±	8.6
					I.A.=	179.0	±	0.5
bot0047	1*	76.5	1.4	14.7	7.9	208.7	±	19.8
	2	29.6	3.8	14.9	6.7	177.5	±	6.5
	3	10.5	12.5	15.3	6.8	181.1	±	1.6
	4	5.9	12.9	15.4	6.7	179.1	±	2.2
	5	11.9	15.1	15.4	6.7	177.6	±	1.8
	6	7.2	16.8	15.7	6.8	181.0	±	1.1
	7	5.1	12.2	15.4	6.9	182.2	±	2.0
	8	7.0	8.4	15.5	6.8	179.8	±	2.6
	fuse	7.4	16.9	15.7	7.0	184.9	±	1.3
					I.A.=	181.2	±	0.7

Table 2

	Step n°	Atmospheric contamination (%)	^{39}Ar (%)	$^{37}Ar_{Ca}/^{39}Ar_{K}$	$^{40}Ar^{*}/^{39}Ar$	Age (Ma)		
bot16	1	49.1	8.2	14.9	7.3	195.1	±	7.1
	fuse	21.9	91.8	21.8	6.8	181.4	±	1.7
					I.A.=	182.5	±	1.6
bot0089	1	30.7	12.2	7.8	6.7	178.8	±	3.5
	fuse	11.8	87.9	8.2	6.7	180.4	±	2.9
					I.A.=	180.2	±	2.6
bot0078	1	52.4	16.6	18.6	6.8	181.9	±	6.0
	fuse	13.9	83.4	19.5	6.7	178.9	±	2.0
					I.A.=	179.4	±	1.9
bot0040	1	56.1	9.9	8.4	7.9	210.5	±	6.3
	fuse	20.3	90.1	13.8	6.9	184.0	±	1.3
					I.A.=	186.6	±	1.3
bot0048	1	42.4	8.2	16.1	6.5	173.4	±	6.7
	fuse	11.7	91.8	16.1	6.9	181.1	±	1.3
					I.A.=	180.5	±	1.3
bot0080	1	21.8	11.1	11.8	6.9	184.5	±	6.8
	fuse	13.0	88.9	15.1	6.7	179.6	±	1.5
					I.A.=	177.7	±	1.5
bot0051	1	55.9	9.2	13.5	6.9	181.7	±	11.2
	fuse	25.5	90.8	17.5	6.8	180.3	±	1.5
					I.A.=	180.5	±	1.7
bot00100	1	64.4	15.0	11.7	6.1	163.8	±	20.3
	fuse	33.4	85.0	12.6	6.5	175.4	±	3.5
					I.A.=	173.3	±	4.3
bot00109	1	88.8	5.0	8.3	6.7	178.1	±	20.8
	fuse	47.0	95.0	9.5	7.0	184.9	±	1.7
					I.A.=	184.6	±	1.9
bot0081	1	49.6	11.1	19.2	6.1	159.7	±	6.2
	fuse	21.9	88.9	22.4	6.9	179.9	±	2.2
					I.A.=	180.1	±	2.1
bot0041	1	32.7	6.2	9.2	6.9	183.8	±	4.5
	fuse	5.3	93.9	11.7	6.8	180.3	±	0.9
					I.A.=	180.5	±	0.9
bot0061	1	74.0	6.1	13.5	7.2	193.3	±	14.9
	fuse	16.6	93.9	16.4	6.7	181.7	±	1.7
					I.A.=	182.4	±	1.8
bot0050	1	53.1	14.6	11.9	7.0	187.9	±	12.4
	fuse	13.1	85.4	17.4	6.9	187.2	±	2.5
					I.A.=	187.3	±	2.8
bot0086	1	91.4	5.0	6.3	3.4	97.1	±	118.8
	2	66.4	10.2	10.7	6.3	175.3	±	37.8
	fuse	52.0	84.8	15.2	6.5	180.0	±	5.6
					I.A.=	173.8	±	5.0
bot00101a	1	92.0	8.0	4.2	7.8	215.8	±	30.5
	2	81.6	13.5	7.1	5.6	157.0	±	17.3
	fuse	39.3	78.6	9.8	7.0	194.9	±	3.3
					I.A.=	191.5	±	4.2
bot0059	1	72.0	10.4	13.0	4.7	127.6	±	33.4
	fuse	19.8	89.6	13.6	6.6	178.8	±	4.1
					I.A.=	175.6	±	5.0
bot0090	1	69.7	13.1	18.7	7.4	196.9	±	27.5
	fuse	32.4	86.9	21.1	6.8	182.3	±	5.0
					I.A.=	184.2	±	5.6

Table 3

Jurassic dykes														
Sample	**Bot02**	**Bot03**	**Bot06**	**Bot07**	**BOT 10A**	**BOT 16**	**BOT 19***	**BOT 20**	**Bot0039**	**Bot0040**	**Bot0041**	**Bot0042**	**Bot0043**	**Bot0044**	**Bot0045**
SiO_2	49.19	50.37	49.66	50.45	49.28	50.60	49.07	48.82	50.25	50.39	49.23	50.31	49.16	48.90	49.15
Al_2O_3	14.42	14.45	13.74	14.00	13.06	16.54	14.64	14.02	13.98	13.85	12.85	12.26	12.96	12.38	12.33
Fe_2O_3	12.88	12.88	13.86	13.95	14.74	10.72	12.37	13.38	12.77	13.02	14.16	13.54	13.31	13.49	13.87
MgO	6.27	5.02	4.83	3.81	5.32	4.92	6.03	5.84	5.98	5.06	5.15	4.66	5.01	4.89	5.13
CaO	10.34	9.71	9.64	8.90	9.59	10.56	10.56	10.36	10.18	9.45	9.14	8.95	9.13	9.16	9.16
Na_2O	2.55	3.15	2.51	3.06	2.58	2.59	2.58	3.22	2.33	2.43	2.40	2.41	2.34	2.22	2.20
K_2O	0.34	0.70	0.97	1.32	0.71	0.96	0.43	0.29	0.65	1.12	1.04	0.88	1.32	1.31	1.44
TiO_2	2.26	2.85	3.48	3.06	3.48	2.18	2.54	2.13	2.50	2.94	3.60	3.73	3.87	4.07	4.09
P_2O_5	0.24	0.32	0.39	0.42	0.39	0.24	0.28	0.24	0.28	0.34	0.42	0.46	0.51	0.51	0.52
MnO	0.18	0.18	0.19	0.15	0.19	0.15	0.18	0.20	0.18	0.16	0.18	0.16	0.17	0.17	0.19
LOI	0.94	1.16	0.92	1.64	0.99	0.61	1.25	1.37	1.00	0.86	1.17	1.84	1.38	1.44	1.07
TOTAL	99.61	100.79	100.19	100.76	100.33	100.07	99.93	99.87	99.52	99.62	99.34	99.2	99.16	98.54	99.15
Mg#	53.15	47.6	44.82	38.89	45.69	51.68	53.19	50.43	52.18	47.53	45.88	44.51	46.73	45.79	46.29
Zr	156	221	254	286	249	157	185	151	191	258	294	353	381	382	388

Jurassic dykes														
Sample	**Bot0046**	**Bot0047**	**Bot0048**	**Bot0049**	**Bot0050**	**Bot0051**	**Bot0053**	**Bot0054**	**Bot0055**	**Bot0056**	**Bot0057**	**Bot0058**	**Bot0059**	**Bot0060'**	**Bot0061**
SiO_2	49.67	49.77	49.67	55.31	48.21	49.43	49.69	49.74	48.97	49.98	49.69	49.45	48.45	49.58	50.04
Al_2O_3	12.95	14.45	14.90	11.83	14.53	13.71	13.18	13.58	15.33	13.29	14.73	14.81	13.66	12.61	13.07
Fe_2O_3	13.57	12.74	12.14	13.43	13.45	12.94	14.16	13.84	11.18	13.31	12.18	12.90	14.01	14.68	14.08
MgO	5.57	3.93	5.08	2.49	5.50	5.96	5.92	5.82	5.95	5.80	7.08	4.06	5.17	5.02	4.96
CaO	9.60	8.67	9.89	5.16	9.64	9.75	9.94	10.29	10.48	10.17	11.02	8.49	9.43	9.51	9.10
Na_2O	2.25	2.77	2.47	3.36	2.67	2.34	2.36	2.45	2.38	2.14	2.17	2.93	2.47	2.39	2.43
K_2O	0.95	1.63	0.97	3.2	0.99	0.97	0.63	0.32	1.13	0.77	0.51	1.70	1.19	0.90	1.19
TiO_2	3.01	3.26	2.74	2.31	2.72	2.81	2.28	2.23	2.29	2.70	2.24	3.44	3.27	3.41	3.34
P_2O_5	0.33	0.59	0.32	0.97	0.30	0.31	0.24	0.24	0.34	0.28	0.25	0.80	0.38	0.39	0.40
MnO	0.17	0.16	0.16	0.18	0.18	0.17	0.20	0.20	0.16	0.19	0.18	0.15	0.18	0.19	0.17
LOI	1.08	1.27	0.74	0.49	1.43	1.51	0.75	0.99	1.54	0.97	0.34	0.79	1.39	0.64	0.91
TOTAL	99.15	99.24	99.08	98.73	99.62	99.90	99.35	99.7	99.75	99.60	100.39	99.52	99.6	99.32	99.69
Mg#	48.89	41.82	49.37	30.17	48.80	51.77	49.35	49.5	55.36	50.39	57.53	42.31	46.24	44.35	45.08
Zr	248	430	247	720	207	226	164	159	236	203	168	486	273	268	279

Jurassic dykes														
Sample	**Bot0062**	**Bot0063**	**Bot0064**	**Bot0065**	**Bot0066**	**Bot0067**	**Bot0068**	**Bot0072**	**Bot0073**	**Bot0074**	**Bot0075**	**Bot0076**	**Bot0077**	**Bot0078**	**Bot0079**
SiO_2	49.11	49.65	49.30	50.06	49.42	48.22	48.40	50.02	49.44	49.84	50.11	49.02	50.10	48.33	50.44
Al_2O_3	12.85	13.76	12.25	13.72	12.15	17.62	15.36	13.41	14.03	13.33	13.72	13.65	13.90	13.62	14.03
Fe_2O_3	14.43	13.05	14.32	12.74	14.93	10.6	12.18	13.75	13.42	13.57	13.17	13.77	12.43	13.76	13.37
MgO	5.39	6.02	4.99	6.22	5.13	4.29	4.64	5.72	5.21	5.34	5.51	5.46	6.43	5.87	4.84
CaO	9.51	10.09	9.33	10.23	9.36	9.91	9.49	10.12	9.83	9.48	9.70	10.16	10.48	8.69	9.60
Na_2O	2.45	2.33	2.27	2.39	2.29	2.93	2.66	2.37	2.41	2.59	2.58	2.54	2.27	3.58	2.23
K_2O	0.94	0.83	1.01	0.51	0.98	1.32	1.43	0.76	0.80	0.59	0.55	0.42	0.58	0.74	0.91
TiO_2	3.07	2.62	3.92	2.59	3.39	3.30	3.55	2.97	2.96	3.49	3.37	3.10	2.46	2.21	2.96
P_2O_5	0.35	0.31	0.46	0.28	0.38	0.52	0.56	0.34	0.33	0.41	0.39	0.35	0.26	0.26	0.35
MnO	0.19	0.18	0.19	0.18	0.20	0.13	0.16	0.19	0.18	0.17	0.17	0.19	0.17	0.19	0.18
LOI	1.22	0.96	1.14	1.05	0.61	0.99	1.73	0.77	1.37	1.01	1.15	1.24	0.86	1.75	0.88
TOTAL	99.51	99.80	99.18	99.97	98.84	99.40	100.16	100.42	99.98	99.82	100.42	99.90	99.94	99.00	99.79
Mg#	46.54	51.81	44.82	53.22	44.47	48.54	47.03	49.23	47.50	47.84	49.37	48.03	54.66	49.85	45.76
Zr	244	217	316	199	267	340	370	221	225	291	269	234	191	170	250

Table 3

	Jurassic dykes														
Sample	**Bot0080**	**Bot0081**	**Bot0082**	**Bot0089**	**Bot0090**	**Bot0091**	**Bot0096**	**Bot0097**	**Bot0098**	**Bot0099**	**Bot00100**	**Bot00101a**	**Bot00102**	**Bot00103**	**Bot00104**
SiO_2	47.93	48.47	50.77	54.13	50.33	50.95	48.97	50.50	49.79	49.79	50.18	49.42	50.26	50.57	50.06
Al_2O_3	13.60	13.66	13.29	13.5	13.89	13.36	12.82	13.20	12.26	13.99	13.11	12.70	14.62	14.53	13.21
Fe_2O_3	13.36	13.38	13.26	13.16	12.02	13.86	14.35	14.44	13.77	12.49	13.71	13.52	12.05	11.87	12.23
MgO	6.53	6.45	5.68	2.40	6.75	5.31	5.24	5.58	5.01	4.52	4.84	4.88	5.56	5.52	4.60
CaO	10.22	9.75	9.96	6.20	10.70	9.71	9.44	9.86	9.00	9.24	8.59	9.35	9.87	10.28	7.50
Na_2O	2.30	2.52	2.24	2.60	2.50	2.52	2.55	2.56	2.29	2.80	2.62	2.33	2.49	2.30	2.68
K_2O	0.68	0.82	0.68	2.51	0.63	0.63	0.67	0.48	1.30	1.08	1.39	1.38	0.97	0.89	2.16
TiO_2	2.44	2.37	2.67	3.48	2.12	3.00	3.60	2.77	3.71	3.88	3.68	4.10	2.20	2.29	4.25
P_2O_5	0.24	0.26	0.30	0.97	0.23	0.34	0.41	0.30	0.42	0.53	0.43	0.53	0.26	0.26	0.57
MnO	0.18	0.19	0.18	0.16	0.18	0.19	0.19	0.20	0.18	0.16	0.17	0.17	0.17	0.18	0.12
LOI	2.02	1.80	0.96	0.82	0.47	0.71	1.03	0.77	0.96	1.5	0.63	1.18	0.95	0.76	2.40
TOTAL	99.5	99.67	99.99	99.36	99.82	100.58	99.27	100.37	98.69	99.22	99.35	98.81	99.40	99.45	99.78
Mg#	53.25	52.91	49.96	29.83	56.69	47.17	45.98	47.38	45.89	45.75	45.14	45.69	51.82	52.01	46.71
Zr	166	184	217	649	157	233	283	199	310	357	298	373	190	202	437

	Jurassic dykes					
Sample	**Bot00105**	**Bot00106**	**Bot00107**	**Bot00108**	**Bot00109**	**Bot00110**
SiO_2	49.75	51.33	49.03	49.78	50.10	49.08
Al_2O_3	12.15	13.48	12.51	12.89	12.83	13.62
Fe_2O_3	13.74	13.37	14.67	14.40	13.93	13.3
MgO	4.09	5.73	5.06	5.49	5.87	6.15
CaO	8.16	9.39	9.52	9.75	9.67	10.35
Na_2O	2.63	2.49	2.35	2.47	2.51	2.45
K_2O	1.38	1.03	0.89	0.52	0.80	0.34
TiO_2	3.89	2.51	3.64	2.61	2.69	2.37
P_2O_5	0.59	0.29	0.40	0.29	0.29	0.25
MnO	0.17	0.17	0.19	0.20	0.18	0.18
LOI	1.82	0.64	0.99	0.57	0.02	0.83
TOTAL	98.37	100.5	99.25	98.97	98.89	98.92
Mg#	40.96	49.97	44.56	47.05	49.55	51.87
Zr	417	205	271	197	208	170

Table 3

Proterozoic dykes and sills											
Sample	**Bot01(s)**	**BOT 11(s)**	**BOT 15A**	**BOT 17**	**Bot0083**	**Bot0084**	**Bot0085**	**Bot0093**	**Bot0094**	**Bot0095**	**Bot0003(s)**
SiO_2	52.06	49.49	48.93	52.39	53.31	54.32	53.95	53.42	53.7	53.65	51.09
Al_2O_3	12.36	16.56	14.43	14.54	14.59	14.13	14.37	13.49	13.75	13.85	15.08
FeOtot	16.36	12.89	15.09	9.95	11.11	11.76	11.54	11.43	12.19	11.96	9.92
MgO	3.91	4.49	5.74	8.2	6.32	4.75	5.2	6.19	4.94	5.15	8.2
CaO	7.84	9.54	9.23	11.09	10.42	8.78	9.36	8.58	8.95	8.92	11.57
Na_2O	2.67	3.13	2.62	1.98	1.86	2.06	2.06	2.29	2.15	2.1	1.68
K_2O	1.39	0.92	0.87	0.63	1.04	1.65	1.39	1.87	1.48	1.69	0.58
TiO2	2.09	1.7	1.85	0.5	0.82	0.97	0.94	0.94	0.96	0.93	0.73
P_2O_5	0.23	0.17	0.2	0.06	0.09	0.12	0.11	0.09	0.11	0.11	0.08
MnO	0.21	0.18	0.21	0.16	0.17	0.17	0.17	0.18	0.19	0.18	0.17
LOI	0.51	0.89	0.62	0.93	0.51	1.14	1.17	1.80	1.35	1.42	0.83
TOTAL	99.63	99.96	99.79	100.43	100.24	99.85	100.26	100.28	99.77	99.96	100.1
Mg#	33.96	42.77	44.96	63.7	54.75	46.48	49.11	55.79	46.65	48.13	63.42
Zr	194	133	170	61	95	138	121	99	129	120	78